Cancer Letters 555 (2023) 216041

Contents lists available at ScienceDirect

Cancer Letters

journal homepage: www.elsevier.com/locate/canlet

Reduction of *Staphylococcus epidermidis* in the mammary tumor microbiota induces antitumor immunity and decreases breast cancer aggressiveness

Giancarla Bernardo [a,1], Valentino Le Noci [a,1], Emerenziana Ottaviano [b,1], Loris De Cecco [c], Chiara Camisaschi [d], Simone Guglielmetti [e], Martina Di Modica [f], Giorgio Gargari [e], Francesca Bianchi [a,g], Serena Indino [a], Patrizia Sartori [a], Elisa Borghi [b], Michele Sommariva [a,f], Elda Tagliabue [f], Tiziana Triulzi [f], Lucia Sfondrini [a,f,*]

[a] *Dipartimento di Scienze Biomediche per la Salute, Università degli Studi di Milano, Via Mangiagalli 31, 20133, Milan, Italy*
[b] *Dipartimento di Scienze della Salute, Università degli Studi di Milano, Via di Rudinì 8, 20142, Milan, Italy*
[c] *Molecular Mechanisms Unit, Department of Research, Fondazione IRCCS - Istituto Nazionale dei Tumori, Via Amadeo 42, 20133, Milan, Italy*
[d] *Biomarkers Unit, Department of Applied Research and Technical Development, Fondazione IRCCS - Istituto Nazionale dei Tumori, Via Amadeo 42, 20133, Milan, Italy*
[e] *Dipartimento di Scienze per gli Alimenti, la Nutrizione e l'Ambiente (DeFENS), Università degli Studi di Milano, Via Mangiagalli 25, 20133, Milan, Italy*
[f] *Molecular Targeting Unit, Department of Research, Fondazione IRCCS - Istituto Nazionale dei Tumori, Via Amadeo 42, 20133, Milan, Italy*
[g] *U.O. Laboratorio di Morfologia Umana Applicata, IRCCS Policlinico San Donato, Piazza Edmondo Malan 2, 20097, San Donato Milanese, Milan, Italy*

ARTICLE INFO

Keywords:
Mammary microbiota
Mammary tumor
Antibiotic
Cancer immunosurveillance
Mouse models

ABSTRACT

The mammary gland hosts a microbiota, which differs between malignant *versus* normal tissue. We found that aerosolized antibiotics decrease murine mammary tumor growth and strongly limit lung metastasis. Oral absorbable antibiotics also reduced mammary tumors. In ampicillin-treated nodules, the immune microenvironment consisted of an M1 profile and improved T cell/macrophage infiltration. In these tumors, we noted an under-representation of microbial recognition and complement pathways, supported by TLR2/TLR7 protein and C3-fragment deposition reduction. By 16S rRNA gene profiling, we observed increased *Staphylococcus* levels in untreated tumors, among which we isolated *Staphylococcus epidermidis,* which had potent inflammatory activity and increased Tregs. Conversely, oral ampicillin lowered *Staphylococcus epidermidis* in mammary tumors and expanded bacteria promoting an M1 phenotype and reducing MDSCs and tumor growth. Ampicillin/paclitaxel combination improved the chemotherapeutic efficacy. Notably, an Amp-like signature, based on genes differentially expressed in murine tumors, identified breast cancer patients with better prognosis and high immune infiltration that correlated with a bacteria response signature.

This study highlights the significant influence of mammary tumor microbiota on local immune status and the relevance of its treatment with antibiotics, in combination with breast cancer therapies.

1. Introduction

In addition to the gut, several organs and tissues that were once considered to be sterile host a distinct microbiota [1]. Recent studies have reported specific changes in the microbiomes of tumoral tissues of various histotypes *versus* their normal counterparts [2] and examined their biological effects on cancers. Notably, in lung and pancreatic cancer, tumor-associated microbiomes affect cancer progression by recruiting immunosuppressive and inflammatory cells that inhibit the antitumor immune response [3–5]. Further, tumor-associated microbiota has direct effects, particularly in colon and mammary tumors, through the release of bacterial toxins and metabolites that damage DNA

* Corresponding author. Dipartimento di Scienze Biomediche per la Salute; Università degli Studi di Milano, Via Mangiagalli 31, 20133, Milan, Italy.
E-mail addresses: giancarla.bernardo@unimi.it (G. Bernardo), valentino.lenoci@unimi.it (V. Le Noci), emerenziana.ottaviano@unimi.it (E. Ottaviano), loris.dececco@istitutotumori.mi.it (L. De Cecco), chiara.camisaschi@humanitasresearch.it (C. Camisaschi), simone.guglielmetti@unimi.it (S. Guglielmetti), martina.dimodica@istitutotumori.mi.it (M. Di Modica), giorgio.gargari@unimi.it (G. Gargari), francesca.bianchi1@unimi.it (F. Bianchi), serena.indino@unimi.it (S. Indino), patrizia.sartori@unimi.it (P. Sartori), elisa.borghi@unimi.it (E. Borghi), michele.sommariva@unimi.it (M. Sommariva), elda.tagliabue@istitutotumori.mi.it (E. Tagliabue), tiziana.triulzi@istitutotumori.mi.it (T. Triulzi), lucia.sfondrini@unimi.it (L. Sfondrini).
[1] These authors contributed equally.

https://doi.org/10.1016/j.canlet.2022.216041
Received 21 June 2022; Received in revised form 16 November 2022; Accepted 18 December 2022
Available online 22 December 2022

and influence tumor growth and migration [6,7]. These data raise the possibility that the tumor-associated microbiome is an active participant in the complex tumor ecosystem [8].

A specific microbiota, potentially originating in the skin, mouth, or gut, has been identified by 16S rRNA gene sequencing in the mammary gland [9]. The female breast is a nutrient-rich environment that comprises fatty tissue with an extensive vasculature, lymphatics, and diffuse lobules and ducts from the nipples—rendering it conducive to the spread of microbes. *Proteobacteria* and *Firmicutes* are the most common bacterial communities in the breast, perhaps due to their association with adiposity and fatty acid-rich environments [10]. The presence of viable bacteria in mammary tissue has also been confirmed by culture, including *Bacillus* sp., *Enterobacteriaceae* sp., and *Staphylococcus* sp [10].

Differences in the microbial composition of the mammary gland have been observed between malignant and normal tissue and benign and malignant tumors [11,12], and notably, distinct microbial signatures have been linked to mammary tumor subtypes [2,13]. These results suggest that changes in microbial communities in the tissue and tumor microenvironment influence the progression of breast cancer (BC) [12].

For example, the growth of *Lactobacillus* spp. correlates with tumor suppression, whereas *Enterobacteriaceae* has been implicated as a detrimental factor that promotes carcinogenesis [11,14]. Urbaniak et al. showed that women with breast cancer harbor more *Bacillus*, *Enterobacteriaceae,* and *Staphylococcus* [11] than healthy individuals and that such species as *Escherichia coli* and *Staphylococcus epidermidis,* isolated from breast cancer patients, induce DNA double-stranded breaks in HeLa cells [11].

Meta-analyses of the breast cancer microbiome have reported *Bacteroides fragilis* in cancerous *versus* normal tissue and its direct activity in breast carcinogenesis through the secretion of a toxin that accelerates tumor growth and metastatic progression [6]. Moreover, *Fusobacterium nucleatum*, an oral anaerobe that translocates hematogenously in other organs, specifically colonizes murine mammary tumors and promotes tumor growth and metastatic progression by suppressing T cells [15,16].

The mammary tumor immune microenvironment is an important determinant of tumor progression. High tumor-infiltrating lymphocyte (TIL) counts are associated with increased sensitivity to chemotherapy in all BC subtypes, reflected by higher pathological complete response rates to neoadjuvant chemotherapy [17]. In addition to their direct cytotoxic effects, immunomodulatory activities have been reported for many chemotherapeutic compounds for BC [18], based on their ability to favor accessibility of the immune system to tumor antigens and danger signals and to activate immune cells. Thus, the nature of the bacteria and bacterial compounds that are produced in or recruited to the mammary tumor might influence cancer cell growth and the response to chemotherapy by modulating its immune microenvironment.

In this study, we demonstrate that oral antibiotic treatment alters the bacterial composition of tumor-associated microbiota in murine mammary tumors, directing the local immune microenvironment toward an antitumor phenotype. Mechanistically, oral antibiotic reduces *Staphylococcus epidermidis levels*, that induces robust inflammation in the tumor, and concomitantly raises under-represented bacteria that favor an antitumor immune response. These changes impair tumor growth and improve the response to paclitaxel in mammary tumors. We also found that in a human breast cancer dataset, a signature that is based on differentially expressed genes between antibiotic-treated and untreated murine tumors identified tumors with a better prognosis and high immune infiltration, that correlated with a signature of response to bacteria. Thus, our findings demonstrate that tumor-residing bacteria shape the mammary tumor immune infiltrate and that strategies to target tumor-associated microbiota should be combined with chemotherapy and immunotherapy in clinical studies to create a favorable immune milieu.

2. Materials and methods

2.1. Cell lines and reagents

The 4T1 (ATCC) and N2C (generated as described [19] and kindly provided by Dr. Colombo) mouse mammary tumor cell lines were routinely maintained at 37 °C in a 5% CO_2 atmosphere in RPMI-1640 (EuroClone) and Dulbecco's modified Eagle's medium (DMEM) (Gibco), respectively, both of which were supplemented with 10% fetal bovine serum (FBS) (Gibco). The cell lines were authenticated by short tandem repeat DNA profiling, and cultures were tested regularly for mycoplasma using the mycoAlert Plus Kit (Lonza). Vancomycin was provided by PharmaTex, and neomycin trisulfate salt hydrate, ampicillin, and paclitaxel were purchased from Sigma-Aldrich (Sigma Aldrich).

Three bacterial species—*Staphylococcus epidermidis*, *Clostridium perfringens,* and *Micrococcus luteus*—used for *in vivo* and *in vitro* experiments, were isolated from 4T1 tumors in mice.

2.2. Mice and experimental protocols

All experiments were performed using 8–12-week-old female BALB/c mice (Charles River) that were maintained in laminar flow rooms at constant temperature and humidity, with food and water given *ad libitum*. Mice were housed under pathogen-free conditions in the animal facility of Fondazione IRCCS Istituto Nazionale dei Tumori. Experiments were approved by the Ethics Committee for Animal Experimentation of Fondazione IRCCS Istituto Nazionale dei Tumori of Milan per institutional guidelines and Italian Law (D-lgs 26/2014). *In vivo* experiments were approved by the Italian Ministry of Health.

BALB/c mice were injected with 5×10^4 4T1 or 1.8×10^5 N2C cells into the mammary fat pad. In all experiments, antibiotics were administered for 3–4 weeks (by aerosol, orally, or peritumorally), starting the day after tumor implantation. For experiments in which treatment was begun in the presence of a palpable tumor nodule, oral antibiotic was started 7 days after tumor injection. Aerosolization was performed 5 days/week using a tower inhalation system (IES 306 Inhalation Towers EMMS). Vancomycin (50 mg) plus neomycin (100 mg) or ampicillin (100 mg) was dissolved in 5 ml saline, and the suspensions were placed in a nebulizer (Aeroneb Lab Micropump Nebulizer) (EMMS), to which groups of 6 mice were exposed for 20 min.

Oral treatment consisted of the administration of vancomycin (0.5 mg/l) plus neomycin (1 g/l), ampicillin (1 g/l), or clindamycin (0.5 g/l), dissolved in 100 ml drinking water, with the biberon changed every 48 h. Peritumoral treatments consisted of 200 μl ampicillin or vancomycin/neomycin, dissolved in 50 μl saline and injected around the tumoral nodule 5 days/week for 4 weeks.

For *in vivo* transfer of bacteria that were isolated from 4T1 tumors, 10^4 CFU of *Micrococcus luteus, Staphylococcus epidermidis,* or *Clostridium perfringens* was injected peritumorally in a 50-μl volume 5 days/week for 7 days, starting on Day 10 after tumor injection and after 10 days of treatment with oral ampicillin. Before administration, the bacterial cells were washed twice in saline, centrifuged at 1900 g for 10 min, and resuspended in fresh saline.

In the combination experiment with oral antibiotic and chemotherapy, paclitaxel was dissolved by adding absolute ethanol and Cremophor ELP (both 5% of the final volume) and administered intraperitoneally at 20 mg/kg once per week, starting on Day 3 after tumor injection.

The antitumor activity of effector immune cells from the lung immune infiltrates was evaluated by measuring the cytotoxic activity of nonadherent cells that were obtained from lung suspensions against ^{51}Cr-4T1 target cells, as described [20]. The radioactivity of the supernatant (80 μl) was measured as described [20].

Tumor growth was monitored every 3–4 days and assessed morphometrically using a Vernier caliper. Tumor volumes were

calculated as V (mm^3) = L (major axis) x W^2 (minor axis)/2.

In all experiments, mice were weighed and inspected for signs of suffering twice per week and euthanized at the end of each experiment. All *in vivo* experiments were repeated at least twice.

2.3. Clonogenic assay in spontaneous lung metastases-bearing mice

To quantify spontaneous lung metastases that were derived from the growth of 4T1 cells in the mammary gland, lungs were removed, digested in DMEM that contained collagenase (300 U/mL) and hyaluronidase (100 U/mL) (StemCell Technologies) for 1 h at 37 °C, filtered through 70-μm cell strainers, and washed twice with 1X PBS. Cells were resuspended in medium that contained 60 μM 6-thioguanine (Sigma Aldrich) and plated in 6-well tissue culture plates at various dilutions. After 14 days, the plates were fixed with methanol, and 6-thioguanine-resistant colonies were stained with 0.03% methylene blue and counted. After dilution factors were accounted for, the data were expressed as the total number of metastatic colonies per organ.

2.4. RNA extraction, reverse-transcription, and quantitative real-time PCR

Tumor samples from mice that bore 4T1 BC cells and were treated with or without aerosolized or oral antibiotics were cut into small pieces and homogenized in QIAzol Lysis Reagent (QIAGEN). Total RNA was isolated according to the manufacturer's instructions, and reverse-transcription was performed using the High-Capacity RNA-to-cDNA™ Kit (ThermoFisher Scientific). Quantitative real-time PCR was performed using TaqMan®Fast Universal PCR Master Mix (ThermoFisher Scientific) on a StepOne Real-Time PCR System (ThermoFisher Scientific).

The following TaqMan® gene expression assays (ThermoFisher Scientific) were used in the real-time PCR analyses: Stat1 (Mm00439531_m1), Stat6 (Mm01160477_m1), Ifnγ (Mm01168134_m1), Il12 (Mm00434169_m1), Ptprc (Mm01293577_m1), Il10 (Mm01288386_m1), Arg1 (Mm00475988_m1), Irf4 (Mm00516431_m1), Irf5 (Mm00496477_m1), Cd69 (Mm01183378_m1), Cd80 (Mm00711660_m1), Cd86 (Mm00444543_m1), Nos2 (Mm00440502_m1), H2-Ab1 (Mm00439216_m1), Ido1 (Mm00492590_m1), and Il6 (Mm00446190_m1). Expression was normalized to β2m (Mm00437762_m1). The PCR data were analyzed using the $2^{-\Delta Ct}$ method.

2.5. In vitro tumor growth assays

The growth of 4T1 cells following antibiotic treatment was evaluated by sulforhodamine B (SRB) assay, as described [21]. Briefly, 1500 cells/well were seeded in a 96-well plate (Costar, Corning Incorporated) in the appropriate growth medium and allowed to attach for 24 h before treatment. The medium was replaced with fresh medium that contained serial dilutions of ampicillin (0–50 μM) in 100 μl/well, and the plates were incubated at 37 °C for 72 h. The cells were then fixed by adding 50 μL/well of trichloroacetic acid (TCA) solution (Sigma Aldrich) for 1 h at 4 °C. Next, the medium was removed, and cells were washed 5 times with deionized water. Following an overnight (ON) airdrying step, 50 μL 0.4% SRB solution was added to each well. After incubation for 1 h at room temperature in the dark, the cells were washed with 1% acetic acid solution and solubilized in 100 μL/well 10 mM Tris base solution (pH 10.5) for 10 min. Absorbance at 490 nm was measured on a spectrophotometer. Differences were considered to be significant at $p < 0.05$.

To determine the effect of antibiotic on 4T1 cell growth in a 3D setting, clonogenic assay in Matrigel (Corning) was performed. Briefly, 4T1 cells were seeded at 3000 cells/well in polymerized Matrigel in triplicate in the presence of various concentrations of ampicillin or control. On Days 5 and 7 of incubation at 37 °C, the colonies were counted under a microscope.

To evaluate the effect of ampicillin directly on 4T1 stem cells, sphere formation test was performed. A total of 3000 4T1 cells/well were seeded in 6-low-attachment-well plates in triplicate with complete MammoCult medium (StemCell Technologies), at various concentrations of ampicillin or control. The cells were incubated at 37 °C for 5 days, and mammospheres were counted under a microscope.

2.6. Flow cytometry

Immune cells in tumor nodules and the spleen were analyzed by FACS. To obtain suspensions of immune-infiltrating cells, tumor nodules were digested in DMEM that contained collagenase (300 U/ml) and hyaluronidase (100 U/ml) (Stemcell Technologies) for 1 h at 37 °C. Cell suspensions were filtered through 70-μm cell strainers (Falcon, Corning), and after red blood cell lysis by incubation in 1x RBC Lysis Buffer Solution (eBiosciences), they were stained for flow cytometric analysis. Splenocyte preparations were obtained by gently flushing the spleen in serum-free RPMI 1640 to release the cells and incubating them in 1x RBC Lysis Buffer Solution, as above. Cells were stained for 30 min at 4 °C using the directly conjugated antibodies in Table 1.

Purified rat anti-mouse CD16/CD32 MAb (eBiosciences, clone 93) was used to block nonspecific binding to mouse Fc receptors. The FOXP3 intracellular staining kit (ThermoFisher Scientific) was used to stain Tregs as described [3], and TLR7 was stained using the FIX & PERM cell permeabilization kit (ThermoFisher Scientific) per the manufacturer's protocol.

The cells were acquired on FACS Celesta and Symphony flow cytometers (BD Biosciences) and analyzed in FlowJo (TreeStar) and Kaluza (Beckman Coulter). All analyses were performed with gating on live $CD45^+$ cells after doublet exclusion.

2.7. Metataxonomic analysis of tissue samples

Tumor nodules of oral ampicillin-treated or untreated mice that were injected with 4T1 tumor cells into the left and right mammary fat pads were collected under sterile conditions and laminar flow. Nodules in the mammary fat pads from one side were harvested for DNA extraction and sequencing of 16S rRNA gene amplicons by Vaiomer (Labège, France), whereas those on the other side were processed to isolate live bacteria, as described below. DNA was extracted from 35 mg of tumor nodules that were frozen immediately after collection, as described [22].

Tissue samples were disrupted using IKA ULTRA TURRAX (Sigma Aldrich); then, a lysis step was performed using acid-washed glass beads (Sigma Aldrich) and a Tissue Lyser (QIAGEN). Finally, DNA was extracted using the QIAamp DNA Stool kit (QIAGEN) and Trizol (ThermoFisher Scientific). Next, a fragment of the 16S rRNA gene that encompassed the V3–V4 variable regions was amplified and sequenced on a MiSeq Illumina system, as described [23]. Pairing, filtering, taxonomic assignment, and taxonomic diversity analyses of the raw amplicon sequencing data were conducted using the bioinformatic pipeline Quantitative Insights Into Microbial Ecology (QIIME), version 1.9.0 [24], and the GreenGenes database (version 13_5).

2.8. Quantification of plasma cytokines

Tumor samples were collected from mice at the end of the experiment and processed according to the manufacturer's instructions. Specifically, tumor samples were weighed in a 2-mL microcentrifuge tube, to which 500 μL Cell Lysis Buffer (ThermoFisher Scientific) was added per 100 mg of tissue. Tubes were assembled into a TissueLyser using 5-mm stainless steel beads (QIAGEN), and tissues were homogenized at 25 Hz for 0.5–3 min. Sample were centrifuged at 16,000 g for 10 min at 4 °C, and the supernatants were transferred to a new microcentrifuge tube. Total protein concentration was measured using the DC Protein Assay Kit (Bio Rad), and samples were diluted to 10 mg protein/mL with

Table 1
List of antibodies for flow cytometry.

Marker	Label	Source	Dilution	Clone	Cat. No.
CD103	BV421	BD	1:100	M290	562771
CD11b	BV510	BD	1:100	M1/70	562950
CD11b	PE-DAZZLE594	BioLegend	1:500	M1/70	101255
CD11c	FITC	MILTENYI	5 μl	N418	130-102-466
CD19	BB515	BD	1:100	1D3	564509
CD25	BV605	BioLegend	1:1000	PC61	102035
CD25	BV650	BD	1:100	PC61	564021
CD3	BB700	BD	1:50	145-2C11	745836
CD3	FITC	MILTENYI	5 μl	145-2C11	130-102-496
CD4	BV510	BD	1:100	RM4	563106
CD4	FITC	BioLegend	1:1000	RM4-5	100510
CD4	Pe/Cy7	ThermoFisher	1:20	GK1.5	25-0041-82
CD44	APC-R700	BD	1:300	IM7	565480
CD45.2	BUV737	BD	1:250	104	564880
CD45	BV786	BD	1:300	30-F11	564225
CD49b	BV421	BD	1:200	HMa2	740030
CD62L	BV650	BD	1:50	MEL-14	564108
CD69	BV786	BioLegend	1:500	H1.2F3	104543
CD69	PE	BD	1:100	H1.2F3	553237
CD8a	APC/Cy7	BioLegend	1:100	53–6.7	100714
CD8	BV605	BD	1:100	53–6.7	563152
CD80	PE	BD	1:100	16-10A1	553769
CD86	APC-R700	BD	1:200	GL1	565479
F4/80	BV711	BioLegend	1:500	BM8	123147
F4/80	BV650	BD	1:100	T45-2342	743282
FoxP3	eF450	ThermoFisher	1:100	FJK-16s	48-5773-82
FoxP3	PE	eBio	1:33	FJK-16s	12-5773-82
LY6C	APC	BioLegend	1:100	HK-1.4	128015
LY6C	APC	BD	1:100	AL-21	560595
LY6G	BUV395	BD	1:500	1A8	563978
LY6G	PE-CF594	BD	1:500	1A8	562700
MHCII	BB700	BD	1:1000	2G9	746086
NKG2D	APC	BD	1:100	CX5	562347
TCRβ	PE/Cy5	BioLegend	1:500	H57-597	109210
TLR2	AF647	BD	1:100	6C2	562625
TLR4	BV650	BD	1:100	MTS510	740615
TLR5	BV421	BD	1:100	ACT5	744164
TLR7	PE	BD	1:100	A94B10	565557
FVS 780		BD	1:1000		565388
Anti Mo CD16/CD32		ThermoFisher	1:100		14-0161-86
LIVE/DEAD Fixable Blue		ThermoFisher	1:2000		L34962

1X PBS and stored at −80 °C until analysis. Cytokines and chemokines were measured using Cytokine & Chemokine 26-Plex Mouse Procarta-Plex™ Panel 1 (ThermoFisher Scientific). Samples were processed according to the manufacturer's instructions and read on a Bio-Plex® 200 (Bio-Rad), as described [25]. Raw fluorescence signals were analyzed and plotted as described [26].

2.9. Histology and immunofluorescence

For histological analysis of lung and liver of 4T1 tumor bearing mice, organs were fixed in 10% neutral buffered formalin for a minimum of 24 h, embedded in paraffin, and sliced (5 μm thick); sections were then stained with hematoxylin and eosin and evaluated by a pathologist.

To determine mastocyte counts, the tumor from each ampicillin-treated or untreated mouse was excised quickly, fixed in formalin, and embedded in paraffin. Sections (5 μm thick) of each sample were deparaffinized in xylene for 10 min and rehydrated in a decreasing series of ethanols. After a final 2-min immersion in distilled water, the sections were stained with 0.1% toluidine blue in 1% sodium borate for 5 min, washed in distilled water, dehydrated through an ascending series of ethanols, cleared with xylene, and coverslipped with resinous mounting medium. Entire sections were acquired on a NanoZoomer S60 digital slide scanner (Hamamatsu Photonics). The total area of sections from each experimental group was calculated in NDP.view 2.8.24 K.K (Hamamatsu Photonics). Each section was examined by 2 blinded operators to identify and count mast cells that were easily identifiable, based on intensely and metachromatically toluidine blue-stained granules. The total number of mast cells in each section was normalized per field (in mm^2) and expressed as mean ± SEM per unit surface area (mm^2).

To measure the deposition of C3 cleavage products (C3b, iC3b, and C3c), tumor sections (5 μm thick) were dewaxed and rehydrated. Antigens were unmasked in 0.01 M citrate buffer, pH 8 solution for 20 min at 90 °C in an autoclave. Autofluorescence was quenched by incubating the tumor sections with 1 M $NaBH_4$ solution in PBS for 10 min at RT. After nonspecific binding sites were saturated with 3% bovine serum albumin (BSA) in 0.1 PBS, pH 7.4 (1 h at RT), the sections were incubated with monoclonal rat anti-mouse C3 (HycultBiotech), diluted 1:20 in 1% BSA/PBS solution (overnight at 4 °C). In the negative controls, the primary antibody was omitted, and C3 was detected using Alexa Fluor 488 goat anti-rat (ThermoFisher Scientific), diluted 1:1000 in 1% BSA/PBS solution (1 h at RT). Nuclei were counterstained with 4′,6-diamidino-2-phenylindole (DAPI) (ThermoFisher Scientific) that was diluted 1:350,000 in distilled water (5 min at RT), and the slides were mounted with ProLong Gold Antifade Mountant (ThermoFisher Scientific).

For quantitative analysis of the C3 immunostaining, 2 sections/mouse from 4 mice/group were analyzed. Two blinded investigators measured the C3-positive area in ImageJ 1.53 in 5 random fields of each section, acquired with constant parameters, on a Leica TCS SP8 X laser scanning confocal microscope (Leica Microsystems GmbH). The results were expressed as the C3-positive area (μm^2) ± SEM.

2.10. Generation of bone marrow-derived macrophages (BMDMs) and stimulation with bacteria

To generate BMDMs, bone marrow cells were harvested from healthy 8-week-old female BALB/c mice (Charles River), as described [27] with slight modifications. Briefly, BM progenitors were harvested from the femur and tibia by fine dissection. Erythrocytes were lysed in ACK Lysing Buffer (ThermoFisher Scientific), and BM cells were cultured in Iscove's Modified Dulbecco's Medium (IMDM) (ThermoFisher Scientific), supplemented with 10% FBS (ThermoFisher Scientific Inc., Waltham, MA, USA), 1% penicillin and streptomycin (ThermoFisher Scientific), and 20 ng/mL macrophage-colony stimulating factor (M-CSF) (PeproTech), in 5% CO_2 at 37 °C.

On Day 3, the culture media was replaced with fresh media that contained M-CSF. BMDMs were harvested after 7 days of M-CSF–mediated macrophage differentiation, after which 5×10^5 BMDMs were plated in 24-well plates, allowed to adhere overnight, and cocultured for 4 h with live *Staphylococcus epidermidis* or *Micrococcus luteus* at a 10:1 ratio. At the end of the incubation, the cultures were washed twice with PBS and centrifuged at 474 g, and RNA was extracted using DirectzolTM RNA MiniPrep (ZYMO RESEARCH). Alternatively, after the wash, the cultures were incubated at 37 °C overnight, and supernatant was collected for Bioplex analysis.

2.11. Isolation of viable bacteria from tumors

Tumors from oral ampicillin-treated and untreated mice were collected under sterile conditions and cut into halves—each of which was incubated overnight in Brain Heart Infusion (BHI) broth and de Man, Rogosa, and Sharpe (MRS) broth, respectively, under anaerobic

and microaerophilic conditions. Twenty-four hours after incubation in broth media, the tumor samples were homogenized, and suspensions were streaked on BHI and MRS agar plates. The plates were incubated under aerobic, anaerobic, and microaerophilic conditions at 37 °C for an additional 24 h. After a CFU count, morphologically distinct colonies were streaked onto new agar plates to obtain pure cultures. Isolated strains were then identified by matrix-assisted laser desorption/ionization time-of-flight (MALDI-TOF) mass spectrometry (BioMerieux VITEK MS).

2.12. ELISA assay

Blood samples (1 ml) from control and treated mice (oral ampicillin, paclitaxel, and oral ampicillin plus paclitaxel) were collected in tubes that contained heparin, and plasma was separated by centrifugation at 2500 rpm for 10 min at 4 °C. Aspartate aminotransferase levels was measured in 6 plasma samples/group, diluted up to 1:320, by Mouse AST ELISA Kit (ab263882 Abcam) according to the manufacturer's protocol. Briefly, 50 µl of standard or sample was added to the well with the appropriate antibody and incubated at room temperature for 1 h. Each well was washed 3 times with 1X Wash Buffer and incubated for 10 min with 100 µl TMB Development Solution. Finally, 100 µl Stop Solution was added, and the OD was measured at 450 nm.

2.13. Gene expression profiling and analyses

RNA was extracted from tumor nodules using the FFPE RNeasy mini kit (QIAGEN). Gene expression profiling was performed by the Genomic Facility of Fondazione IRCCS Istituto Nazionale dei Tumori, Milan. After RNA extraction, a quality check and quantification were performed on a 4200 TapeStation (Agilent) and a Qubit fluorometer using the Qubit RNA HS assay kit (ThermoFischer Scientific), respectively. RNA expression was assessed using the mouse Affymetrix Clariom S Pico assay (ThermoFisher Scientific). A total of 100 ng of total RNA was used to generate the single-stranded cDNA samples for hybridization. Then, the cDNA was fragmented enzymatically and biotinylated using the WT Terminal Labeling kit (ThermoFisher Scientific), combined with hybridization buffer, and applied to human Clariom S arrays, which targeted >20,000 well-annotated genes. The arrays were stained on an Affymetrix® GeneChip® Fluidics Station 450 and scanned on a 7G Affymetrix® GeneChip® Scanner 3000.

Raw data were processed using TAC, v4.2.0 (ThermoFisher Scientific). CEL files that contained feature intensity values were converted into summarized expression values by robust multiarray average (RMA), which consists of background adjustment and quantile normalization across all chips. All samples passed the QC thresholds for hybridization, labeling, and the expression of housekeeping gene controls. The data have been deposited into the Gene Expression Omnibus Repository (accession number: GSE205169)

Gene set enrichment analysis was performed using GSEA v4.0.3 [28] on the REACTOME database v7.4 (974 gene sets were used in the analysis) and on a curated bacteria-related database obtained from GO BP, KEGG, and REACTOME, using the keywords "bacteria," "parasite," and "pathogen" (12 gene sets were used in the analysis). Gene set permutation type was applied 1000 times, and gene set enrichment was considered significant at FDR < 10%. Cytoscape v3.8.0 and Enrichment Map were used to visualize the GSEA results as a network of enriched gene sets ($p < 0.05$, FDR < 0.1). Nodes that represented enriched gene sets were grouped and annotated using Cluster Maker and AutoAnnotate apps, based on their similarity. Node size is proportional to the total number of genes in each gene set.

A binary prediction signature for amp-treated mice (amp/untreated) was developed using logistic Least Absolute Shrinkage and Selection Operator (LASSO) regression, a penalized method for estimating a logistic regression model when the number of features (ie, genes) is much greater than the number of samples [29]. Regression coefficients are calculated for all genes to minimize a weighted average of mean squared prediction error for the training set, assigning zero coefficients to genes that are less informative. The weighting factor is optimized by cross-validation to avoid the overfitting.

Publicly available data in the METABRIC dataset were retrieved from https://ega-archive.org/, and after mapping the human ortholog of our LASSO signature, the model was applied to gene expression data. Patients with the highest (n = 53) and lowest scores (n = 192) were stratified as untreated-like and Amp-like tumors, respectively, and used for further analyses. These 2 groups of patients closely resembled the signature thresholds in untreated and amp-treated mouse tumors. The CIBERSORTx web tool (https://cibersortx.stanford.edu/) was used to infer the relative abundance of the immune cell infiltrate using the LM22 matrix to deconvolve the Metabric dataset with 1000 permutations. ssGSEA v10.0.1 was applied with previously published immune scores [30] and curated bacteria-related gene sets.

2.14. Statistical analysis

Differences between groups were compared by two-tailed unpaired student's t-test and were significant at $p \leq 0.05$. All analyses were performed using GraphPad Prism for Windows, version 5.0 (GraphPad Software). The metataxonomic data were analyzed in R (version 3.4.2). Significantly different taxonomic units between groups of samples were determined by differential gene expression analysis, using the negative binomial distribution method (R/Bioconductor DESeq2 package) [31], followed by Welch's *t*-test, with FDR-adjusted p values [31] (padj = 0.05 was used as the threshold for significance). Association among categorical variables was tested by Fisher's exact test. The strength of an association between continuous variables was assessed using the Pearson correlation coefficient (r). Two-sided $p < 0.05$ was considered significant. Survival curves were estimated by Kaplan–Meier method. Cox proportional hazard regression models were used for the univariate and multivariate survival analysis, and hazard ratios (HRs) and their 95% CIs were used to quantify the effects of explanatory variables on event hazards.

3. Results

3.1. Aerosolized antibiotics decrease lung metastases and impair primary mammary tumor growth

In a mouse model of lung metastasis, we have shown that the local microbiota can be altered by antibiotics to dampen the immunosuppressive microenvironment and promote cancer immunosurveillance [3]. In the current study, we examined whether repeated aerosolization of vancomycin/neomycin, which target gram-positive and gram-negative bacteria, beginning on Day 1 from orthotopic implantation of 4T1 mammary carcinoma cells into the mammary fat pad, protects mice from spontaneous metastasis to the lung. Antibiotic aerosolization significantly decreased the growth of metastases in the lung by 82.4% at 4 weeks after orthotopic tumor implantation, by clonogenic assay of cells from lung suspensions, compared with untreated animals (Fig. 1A). Unexpectedly, antibiotic treatment limited the growth of tumor cells that were implanted into the mammary gland (27.7% inhibition) (Fig. 1B). This inhibition was associated with the modulation of immune-related genes. Cd45, Ifnγ, Cd69, and Cd86 mRNA levels were significantly upregulated in the mammary tumors of mice that were aerosolized with vancomycin/neomycin (Fig. 1C). The levels of Il12 and Irf5, an M1 transcription factor, were higher in antibiotic-treated tumors, but Nos2 and Stat1, other M1 markers, were unchanged (Fig. 1C). The upmodulation of certain M1 markers was paralleled by the downregulation of M2 markers in antibiotic-treated tumors, such as Il10, Arg1, Irf4, and Stat6 (Fig. 1C).

In addition to corroborating our previous data on the effects of aerosolized antibiotics in reducing metastases in the lung, as we

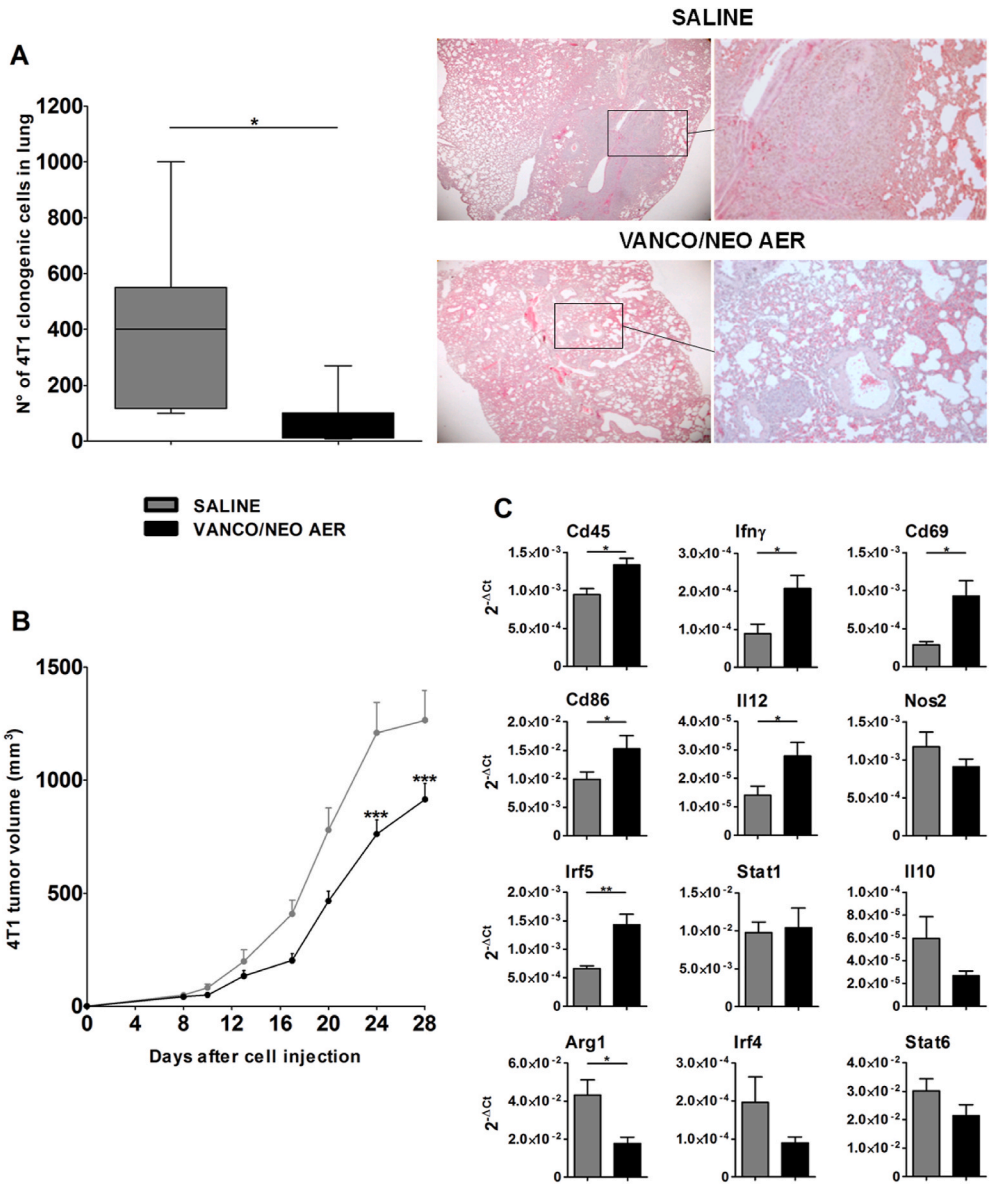

Fig. 1. Effect of vancomycin/neomycin aerosol on 4T1 lung metastases and mammary tumors.
Mice were injected with 4T1 tumor cells into the mammary fat pad and left untreated or treated with aerosolized vancomycin/neomycin, starting 1 day after tumor implantation (7 mice/group). **(A)** Number of lung metastatic colonies by clonogenic assay of lung suspensions collected on Day 28 (mean ± SEM); representative images of 4T1 lung metastases by hematoxylin and eosin at 2x and 10x magnification (inset) are shown. **(B)** Primary mammary tumor growth, expressed as tumor volume (mean ± SEM). **(C)** Mean relative expression ± SEM of Cd45, Ifnγ, Cd69, Cd86, Il12, Nos2, Irf5, Stat1, Il10, Arg1, Irf4, and Stat6 by quantitative RTqPCR in mammary tumor nodules on Day 28. Results are presented as $2^{-\Delta Ct}$ using β2m as reference. *p ≤ 0.05, **p ≤ 0.01, and ***p ≤ 0.001.

observed for melanoma cells [3], these results provide evidence that antibiotic treatment impedes the growth of mammary tumors by favoring a local antitumor immune microenvironment, constituting a springboard for our study.

3.2. *Absorbable oral antibiotics reduce mammary tumor growth and affect the local immune microenvironment*

To further examine the effects of antibiotics on mammary tumor growth, we compared the oral and aerosol administration of vancomycin/neomycin, which minimally enter the bloodstream through the intestinal mucosa. Moreover, we determined the effects of oral and aerosol delivery of ampicillin, a wide-spectrum antibiotic against gram-positive and gram-negative bacteria that, unlike vancomycin/neomycin, can cross the small intestinal epithelial barrier.

In contrast to the significant impairment in orthotopically implanted 4T1 mammary tumor growth that was induced by aerosolized vancomycin/neomycin, no effect was observed when these antibiotics were dissolved in drinking water and administered, starting 1 day after tumor implantation (Fig. 2A), whereas ampicillin significantly reduced mammary tumor growth on oral and aerosol administration (Fig. 2A). Notably, 3 cycles of peritumoral administration of ampicillin over 5 days from Day 1 also significantly inhibited 4T1 tumor growth (Fig. 2B). Through this route, vancomycin/neomycin also significantly reduced tumor growth, suggesting that suppression of mammary tumors by antibiotics relies on a direct local effect on mammary tissue.

Greater impairment was effected by oral *versus* aerosol ampicillin. Ampicillin in drinking water reduced 4T1 tumor growth even when administered 7 days after tumor injection in the presence of a palpable tumor nodule (Fig. 2C).

Mammary tumor growth was also impeded by oral ampicillin in mice when N2C tumor cells were implanted into the mammary fat pad, a mammary carcinoma model that has been derived from BALB-NeuT mice, indicating that the antitumor activity of this treatment is not limited to the 4T1 model (Fig. 2D). A similar decrease in 4T1 growth was induced by clindamycin, another broad-spectrum antibiotic that passes the intestinal barrier to become systemically available (Fig. 2E), supporting that the impairment in mammary tumor growth is related to the access of antibiotic to the bloodstream.

4T1 cell viability was unaffected by *in vitro* ampicillin treatment, by SRB assay (Suppl. Fig 1A) and Matrigel clonogenic assay (Suppl. Fig. 1B and 1C), after 48-h exposure to many doses. Moreover, no inhibition of

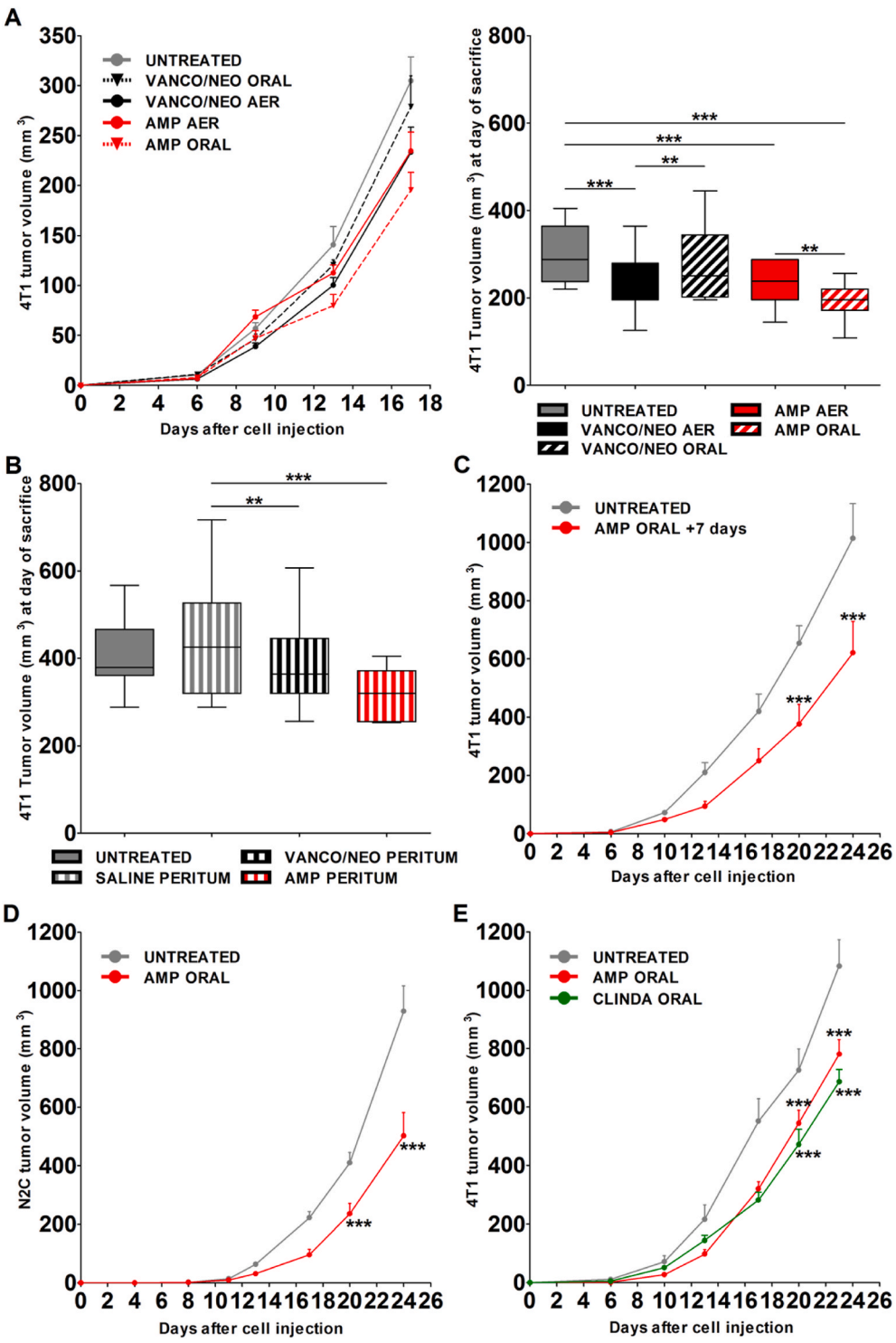

Fig. 2. Effect of vancomycin/neomycin and ampicillin through various routes on mammary tumor growth.
In 2 separate experiments, mice were injected with 4T1 tumor cells into the mammary fat pad and left untreated or treated with vancomycin/neomycin or ampicillin starting 1 day after tumor implantation by aerosol route or orally **(A)** and peritumorally **(B)**, respectively (8–10 mice/group). Primary mammary tumor growth is expressed as tumor volume during the experiment in A or on the day of sacrifice (Day 17 in A and Day 20 in B). Mice were then injected into the mammary fat pad with **(C)** 4T1 tumor cells and untreated or treated with oral ampicillin starting 7 days after tumor injection (8–9 mice/group), **(D)** N2C tumor cells and untreated or treated with oral ampicillin starting 1 Day after tumor injection (8–9 mice/group), and **(E)** 4T1 tumor cells, untreated or treated with oral ampicillin or oral clindamycin starting 1 day after tumor injection (8–9 mice/group). $^{**}p \leq 0.01$ and $^{***}p \leq 0.001$.

mammosphere formation was observed (Suppl. Fig 1D). These results demonstrate no direct effect of ampicillin on the growth of 4T1 cells.

By RT-qPCR of RNA from mammary tumor nodules, Cd45, Ifnγ, and Cd86 were significantly upregulated in tumors from oral ampicillin-treated mice (Fig. 3). Further, M1 markers, including Nos2, Stat1, Irf5, and Il12 (Fig. 3), were upmodulated in these animals. The expression of M2 markers was unchanged. No significant modulation of these genes was detected in the tumors of oral vancomycin/neomycin-treated mice, except for a slight increase in Cd80 and Il12 (Fig. 3).

Changes in tumor-infiltrating immune cells in oral ampicillin-treated mice were analyzed by flow cytometry. Consistent with the results above, the percentage of $CD45^{+}$ cells was higher in ampicillin-treated tumors *versus* saline (Fig. 4A). This expansion was related to a significant increase in the frequency of T cells and macrophages (Fig. 4A), whereas ampicillin treatment correlated with fewer B cells in the tumor microenvironment. No other immune cell populations, including DC subsets, NK cells, and Tregs, were modulated.

Further, based on emerging evidence of mast cells (MCs) as drivers of tumor progression in the breast cancer microenvironment [32], MC levels were analyzed in FFPE tumor tissue from antibiotic-treated and

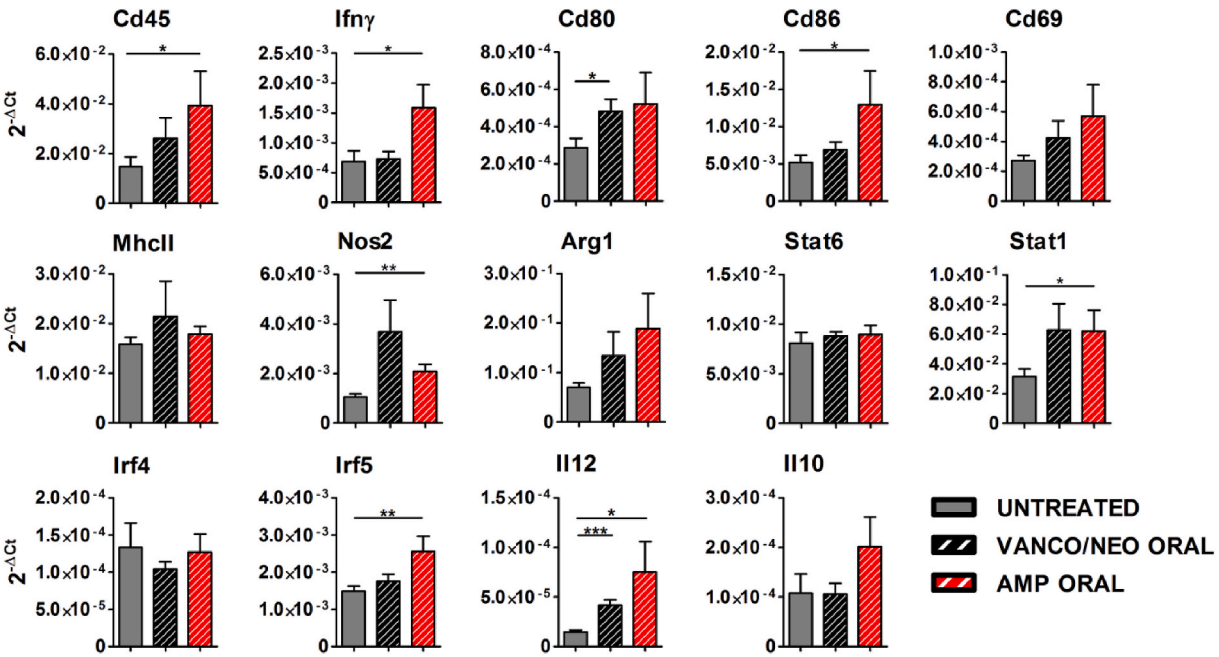

Fig. 3. Effect of oral treatment with vancomycin/neomycin and ampicillin on mammary tumor microenvironment.
Quantitative RT-qPCR of RNA from mammary tumor nodules of mice injected with 4T1 tumor cells into the mammary fat pad and left untreated or treated with oral vancomycin/neomycin or ampicillin from day 1 after tumor implantation (8–10 mice/group). Mean relative expression ± SEM of Cd45, Ifnγ, Cd80, Cd86, Cd69, MhcII, Nos2, Arg1, Stat6, Stat1, Irf4, Irf5, Il12, and Il10 mRNA is expressed as $2^{-\Delta Ct}$. *p ≤ 0.05, **p ≤ 0.01, and ***p ≤ 0.001.

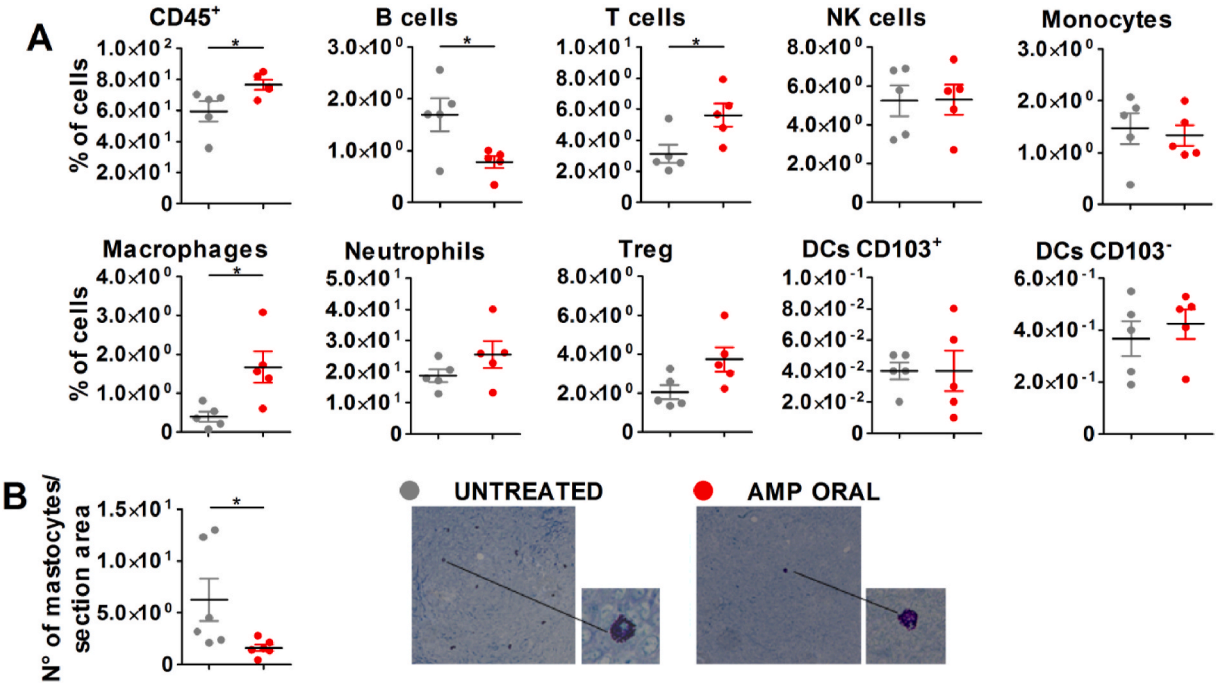

Fig. 4. Effects of oral ampicillin on immune cells infiltrating 4T1 mammary tumors.
(A) Percentage of $CD45^+$ cells, B cells ($CD19^+$), T cells ($CD3^+$), NK cells ($CD3^-CD49b^+$), monocytes ($Ly6c^+F4/80^{int}$), macrophages ($Ly6c^-F4/80^+$), neutrophils ($Ly6g^+CD11b^{hi}$), Tregs ($CD4^+CD25^+FoxP3^+$), $CD103^+$ DCs ($CD103^{++}MHCII^{++}CD11c^+CD11b^{int}$), and $CD103^-$ DCs ($CD103^-MHCII^{int}CD11c^+CD11b^{int}$) by FACS analysis of suspensions from digested tumor nodules of mice injected with 4T1 tumor cells, untreated or treated with oral ampicillin from Day 1 (5 mice/group). Gating strategies are shown in Suppl. Fig. 2. **(B)** Mean number ± SEM of mastocytes/section area of formalin-fixed paraffin-embedded tumors from mice injected with 4T1 tumor cells, untreated or treated with oral ampicillin from Day 1 (6 mice/group). Representative light microscopy images of tumor sections stained with toluidine blue (40X). Toluidine blue stains mastocytes metachromatically in red-purple and the background in blue. In the untreated tumor, mastocytes are visible; an enlarged frame shows a single mastocyte with a pale-stained nucleus. In an ampicillin-treated tumor, a single mast cell is identifiable and enlarged in the frame. Granules obscure the nucleus. *p ≤ 0.05.

untreated mice by toluidine blue staining. MC numbers declined significantly in ampicillin-treated tumors (Fig. 4B).

Together, these results suggest that the impairment of 4T1 mammary tumor growth by antibiotics depends on the systemic bioavailability of antibiotics and demonstrate that the reduced mammary tumor growth is associated with the modulation of the immune microenvironment toward an antitumor phenotype.

3.3. The transcriptomic profile of tumors from oral ampicillin-treated mice is associated with altered microbial signaling

To analyze the effects of ampicillin treatment on tumors at the molecular level, we determined the comprehensive gene expression profile of tumor specimens from ampicillin-treated and untreated tumors. By Gene Set Enrichment Analysis (GSEA), all gene sets that reached the threshold of significance (FDR < 0.10) (415 of 974) were enriched in untreated mice, and no significant gene sets were enriched in the ampicillin-treated group. As shown in Suppl. Table 1 and Fig. 4A,

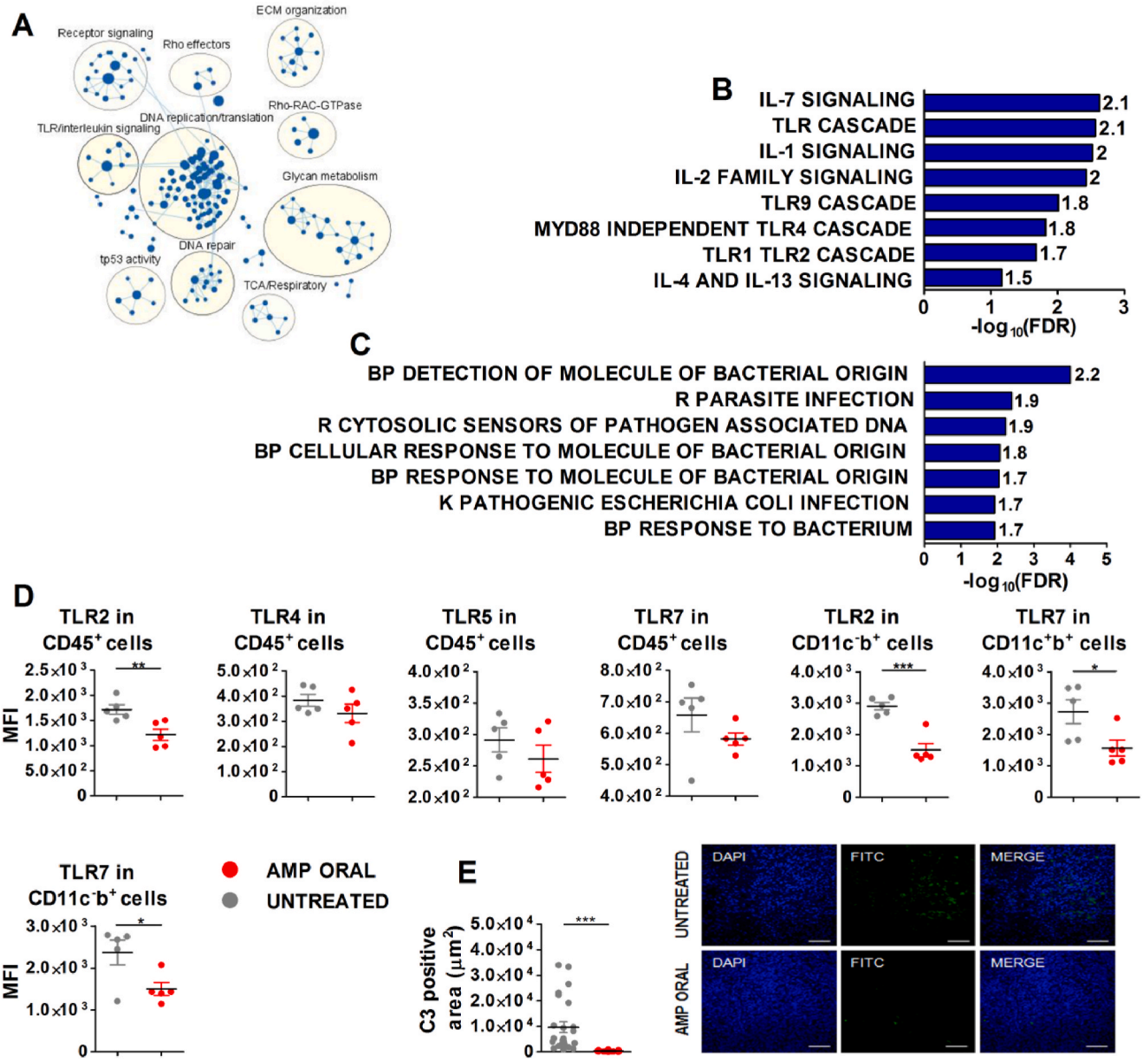

Fig. 5. Effects of oral ampicillin on the transcriptomic profile of 4T1 mammary tumor nodules

(**A**) Enrichment Map of Reactome pathways that are significantly enriched ($p < 0.05$, FDR <0.1) in tumors of untreated versus oral ampicillin-treated mice. Clusters of significantly enriched **(B)** TLR/interleukin signaling gene sets and **(C)** bacteria-related gene sets (FDR<0.1) by Gene Set Enrichment Analysis (GSEA) of 4T1 tumor samples of oral ampicillin-treated versus untreated mice (5–6 mice/group). Normalized enrichment score for each pathway is shown on the right of each column. **(D)** Expression of TLR 2, 4, 5, and 7 by FACS analysis of suspensions of digested 4T1 mammary tumor nodules from mice untreated or treated orally with ampicillin (5 mice/group). Data are expressed as mean fluorescence intensity (MFI) of each TLR in $CD45^+$ and $CD11c^-b^+$ and $CD11c^+b^+$ fractions. Gating strategies are shown in Suppl. Fig. 3. **(E)** Quantification of C3 fragment-positive areas and representative immunofluorescence photomicrographs of tumor sections from mice injected with 4T1 tumor cells, untreated or treated with oral ampicillin (4 mice/group). Sections were stained for C3 cleavage products (C3b, iC3b, and C3c; green), and nuclei were counterstained with 4′,6-diamidino-2-phenylindole (DAPI; blue). Each dot represents the mean C3-positive area (μm^2) in 2 sections/mouse. Results are expressed as mean C3-positive area ± SEM. The C3-positive area was measured in 5 random fields using constant parameters. Bars: 40 μm *$p \leq 0.05$, **$p \leq 0.01$, and ***$p \leq 0.001$.

untreated tumors were enriched primarily in pathways that are involved in cell growth and metabolism and to signaling molecules that regulate cellular responses, supporting the antibiotic-driven impairment of tumor growth. Notably, a cluster of gene sets that were related to pattern recognition receptors (PRRs)—specifically TLRs and interleukin signaling—was also significantly enriched in untreated *versus* ampicillin-treated tumors (Fig. 5A and B).

Similarly, analyzing bacteria-related gene sets, we found that all gene sets that had an FDR <0.10 (7/12) were enriched in the untreated group (Fig. 5C).

Consistent with these data, the $CD45^+$ fraction of tumors from ampicillin-treated mice revealed changes in the expression levels of some TLRs compared with untreated mice (Fig. 5D). Specifically, TLR2, which recognizes bacterial diacyl and triacylglycerol moieties, proteins, and polysaccharides, was downregulated, and TLR7, which recognizes microbial ssRNA, decreased slightly. Among these cells, TLR2 expression was lower in the $CD11c^-CD11b^+$ subset, which includes granulocytes, monocytes, and macrophage-myeloid cells (Fig. 5D). Also, TLR7 decreased significantly in the $CD11c^-CD11b^+$ and $CD11c^+CD11b^+$ fractions, which also contained various myeloid cell populations, including DCs (Fig. 5D). No significant change in other populations was detected (Suppl. Fig. 4A).

TLRs levels were unchanged in the $CD45^-FSC^{high}$ fraction of tumor nodule suspensions in ampicillin-treated *versus* untreated mice (Suppl. Fig. 4B), as well as in $CD45^+$ splenocytes (Suppl. Fig. 4C), suggesting that variations in TLRs on tumor immune-infiltrating $CD45^+$ cells reflect a local change in the tumor-associated microbiota.

Notably, DNA repair was among the gene sets that were significantly enriched in untreated *versus* ampicillin-treated tumors (Fig. 5A). Modulation of this pathway might also be related to changes in the microbiota in the tumor, based on findings that microbial signals alter genes that mediate DNA repair [33].

Similarly, the hypothesis of an effect of antibiotics on the local microbiota was confirmed by the observation that the complement activation pathway, reported to be influenced by the composition of the microbiota [34], was enriched in untreated *versus* ampicillin-treated mice in the Reactome (NES = 1.59, padj = 0.043) and KEGG (NES = 1.52, padj<0.001j) databases. Accordingly, analyzing the deposition of C3 cleavage products by immunofluorescence, we observed significant reductions in C3b, iC3b, and C3c in 4T1 tumors from oral ampicillin-treated compared with untreated mice (Fig. 5E).

Overall, these data suggest that oral ampicillin treatment is associated with changes in microbial signaling in mammary tumoral tissue.

3.4. Oral ampicillin influences the mammary tumor-associated microbiota

To analyze the effects of oral ampicillin on tumor-associated microbiota, we performed 16S rRNA gene profiling of healthy and tumoral mammary samples.

The presence of a distinct bacterial community structure was confirmed in untreated 4T1 tumors that were grown in the mammary fat pad of BALB/c mice (n = 6) *versus* healthy mammary glands (n = 6). As shown in Fig. 6A, OTU richness and Shannon index scores rose significantly by α-diversity analysis in healthy *versus* untreated tumor tissue; the 2 groups of samples were separated, based on intersample diversity, as assessed by unweighted UniFrac distance (PERMANOVA p = 0.019) (Fig. 6B). Accordingly, an analysis of single taxonomic units demonstrated that 19 taxa, belonging to 4 phyla (Actinobacteria, Bacteroidetes, Firmicutes, and Proteobacteria) were enriched in the healthy mammary gland, whereas an undefined genus of the family Intrasporingiaceae (Actinobacteria) was only found in tumor samples (Fig. 6C).

Comparing ampicillin-treated tumors *versus* healthy tissue, α-diversity was similar, whereas the difference in β-diversity, calculated by unweighted UniFrac distance (PERMANOVA P = 0.081), nearly reached significance (Fig. 6A and B). Neither α-diversity nor β-diversity analysis significantly distinguished the tumor samples by antibiotic treatment (Fig. 6A and B). Notably, the concentration of 16S rRNA gene copies did not change significantly by antibiotic treatment (1.01e+007 ± 3.4 e+006 in untreated *versus* 7.18e+006 ± 1.2 e+006 in ampicillin-treated tumors; p = 0.44). Nevertheless, in the analysis of the presence and relative abundance of single taxonomic units, 8 taxa differed significantly, 2 of which were overrepresented in the tumors of untreated mice: an undefined genus of the family Intrasporangiaceae and the genus *Staphylococcus* (Fig. 6D). Conversely, the genus *Corynebacterium*, an undefined genus of the family Micrococcaceae, and an undefined genus of *Comamonadaceae* were enriched in the tumors of ampicillin-treated mice (Fig. 6D).

In parallel, microbial isolates were obtained from untreated and ampicillin-treated tumors that were homogenized under sterile conditions and identified to the species level by MALDI-TOF. The microbial isolates from the tumors of the 2 groups were assigned taxonomically to the species *Staphylococcus epidermidis*, *Bacillus circulans*, *Bacillus cereus*, *Clostridium perfringens,* and *Micrococcus luteus* (Fig. 6E). The total CFU count for *S. epidermidis* (phylum Firmicutes, family Staphylococcaceae) also decreased in homogenized ampicillin-treated *versus* untreated tumors, albeit insignificantly, whereas certain bacteria, such as *Clostridium perfringens* (phylum Firmicutes, family Clostridiaceae) and *Micrococcus luteus* (phylum Actinobacteria, family Micrococcaceae), were isolated only from amp-treated tumors (Fig. 6E).

These results are consistent with the metataxonomic analysis, which demonstrated the overrepresentation of the genus *Staphylococcus* in untreated tumors and of a member of the family Micrococcaceae in the tumors of ampicillin-treated mice.

Based on 16S rRNA gene profiling of taxa to which the other isolated species belonged, the taxonomic units that were assigned to the family Clostridiaceae were present in 4 ampicillin-treated samples (5467 reads detected) compared with 2 untreated samples (2134 total reads detected). In contrast, no taxonomic unit that was assigned to the family Bacillaceae was seen in the metataxonomic profiles (data not shown).

Overall, these results indicate that oral ampicillin treatment affects the composition of the mammary tumor-associated microbiota.

3.5. Effects of 4T1 tumor-isolated bacteria on immune activation

To determine the immunological effects of the bacteria that were isolated from 4T1 tumors and significantly differential between ampicillin-treated and untreated tumors by metataxonomic analysis, BALB/c BMDMs were cocultured for 4 h with live *S. epidermidis,* a facultative anaerobic bacterium, and *M. luteus,* a microaerophilic bacterium, at a ratio of 10:1 bacteria/BMDM. *C. perfringens* was not included in this analysis, given its strict anaerobic metabolism.

S. epidermidis and *M. luteus* upregulated inflammatory cytokine genes in BMDMs, such as Il6 and Il12—a response that was more robust with *S. epidermidis* (Fig. 7A). With regard to transcription factors that were induced in macrophages by the 2 bacteria, *S. epidermidis* upmodulated Irf4, which is linked to the M2 phenotype; in contrast, *M. luteus* significantly increased Irf5 and Stat1, which are typically associated with the M1 profile (Fig. 7A). *M. luteus* downregulated the M2-related Ido1 and upregulated Cd80 and MhcII, which correlate with the M1 profile (Fig. 7A). By Bioplex analysis of culture supernatants of macrophages that were stimulated with bacteria, *S. epidermidis* elicited robust secretion of proinflammatory cytokines (IL1β, IL6, IL12, IL18, and TNFα) and chemokines (MCP1, MIP1α, MIP2, RANTES, EOTAXIN, and GROα) (Fig. 7B). In contrast, these factors were slightly upregulated by *M. luteus*, which significantly modulated only IL12 and RANTES (Fig. 7B).

Based on data that certain strains of *S. epidermidis* are potent inducers of inflammation through complement activation [35], we examined the ability of an *S. epidermidis* strain that was isolated from 4T1 tumors to promote C3 cleavage *in vivo*. High deposition of C3-derived fragments was detected in tumors of mice that were treated for 10 days with oral

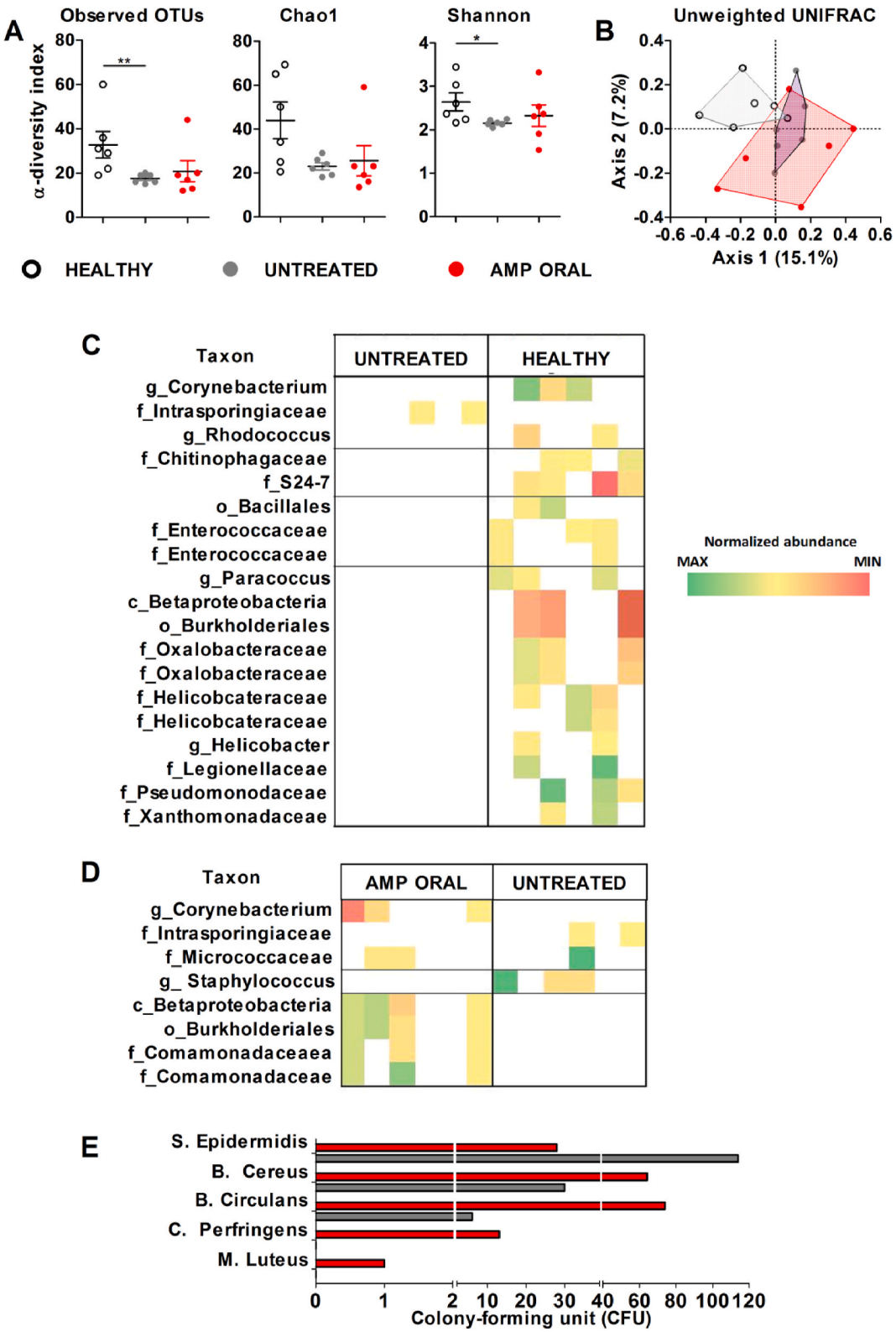

Fig. 6. Effects of oral ampicillin on 4T1 mammary tumor-associated bacterial communities.
(**A**) Intrasample (α) diversity analysis, based on OTUs, Chao1, and Shannon indexes. *$p \leq 0.05$, **$p \leq 0.01$, by Mann–Whitney U (unpaired) test, and (**B**) intersample (β) diversity, represented by multidimensional scaling (MDS) ordination, based on unweighted UniFrac distances, describing ecological diversity. Significantly different bacterial taxa between untreated and healthy mammary gland (**C**) and between ampicillin-treated and untreated tumors (**D**) by DESeq2 normalization (6 mice/group) are shown. Heat map indicates the normalized levels of significantly different taxa per sample; white boxes indicate that the taxon was not detected in the specific sample. **(E)** Tumor nodules of mice injected with 4T1 tumor cells, untreated or treated with oral ampicillin (6 mice/group), were collected under sterile conditions, incubated overnight in broth, homogenized, and cultured on agar plates under aerobic, anaerobic, and microaerophilic conditions. Individual colonies on agar were subcultured and identified to the species level by MALDI-TOF. Total colony forming units (CFUs) from 6 tumors/group are shown.

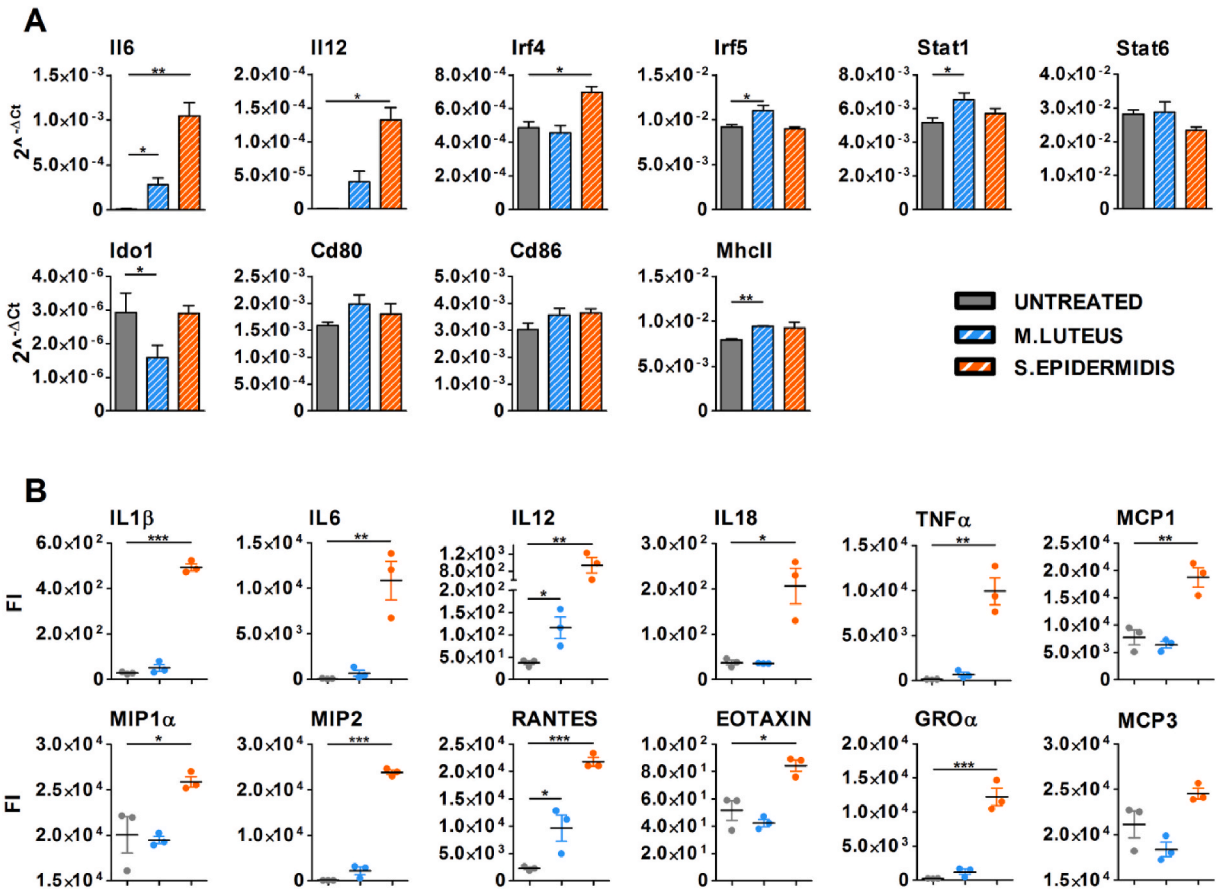

Fig. 7. Effects of bacterial isolates from 4T1 tumor on *in vitro* cultured BMDCs.
(A) RT-qPCR of RNA from macrophages that were differentiated from BALB/c BMDCs cocultured for 4 h with live Staphylococcus epidermidis or Micrococcus luteus (10:1) in triplicate. Mean relative expression ± SEM of Il6, Il12, Irf4, Irf5, Stat1, Stat6, Ido1, Cd80, Cd86, and MhcII is expressed as $2^{-\Delta Ct}$. **(B)** Bioplex analysis of supernatants of BMDMs cocultured for 4 h with bacteria as in A and then for an additional 12 h after a wash step and the addition of fresh media. Fluorescence signals ± SEM of IL1β, IL6, IL12, IL18, TNFα, MCP1, MIP1α, MIP2, RANTES, EOTAXIN, GROα, and MCP3 are shown.

ampicillin and then injected intratumorally with 10^4 CFU *Staphylococcus epidermidis* for 7 days (Fig. 8A), in contrast to minimal deposition with injection of 10^4 CFU *M. luteus*, similar to the level in control mice. Consistent with its low inflammatory activity and ability to stimulate an M1 profile, levels of granulocytic and monocytic MDSCs—hallmarks of the 4T1 tumor microenvironment [36]—decreased only in tumor suspensions from mice that were injected intratumorally with *M. luteus* (Fig. 8B). These cells were not significantly affected in tumors that were injected with *S. epidermidis,* but in these tumors, the levels of CD69-expressing FoxP3+ Tregs, a subset with strong suppressive ability, rose [37] (Fig. 8B).

These results suggest that inhibition of tumor growth by oral ampicillin is related to a decrease in inflammatory/suppressive bacteria in the tumor and the appearance of immune-activating bacteria. In support of this model, *in vivo* transfer of *M. luteus* to implanted 4T1 tumors significantly reduced the size of the tumor nodules compared with the intratumoral saline-treated group (Fig. 8C). No significant change in tumor growth was seen in mice in which tumors received *S. epidermidis* (Fig. 8C). Notably, *in vivo* transfer of *C. perfringens*, which also expanded in tumors from oral ampicillin-treated mice, impeded 4T1 cell growth similarly to *M. luteus* (Suppl. Fig. 6).

3.6. Oral ampicillin improves the efficacy of paclitaxel by increasing its antitumor immune activity

Based on the ability of oral ampicillin to stimulate an antitumor immune microenvironment by modulating the local microbiota, we studied the effect of its combination with paclitaxel, a chemotherapeutic drug with immunostimulatory activity for breast cancer patients that did not have any antitumor effect in the 4T1 model (Suppl. Fig. 7). In addition to arresting the cell cycle by acting on microtubules, this compound promotes antitumor immunity by stimulating TLR4, a lipopolysaccharide-specific receptor that is not affected by ampicillin, and by skewing tumor-associated macrophages (TAMs) toward an immunocompetent profile [38].

Mice were orthotopically implanted with 4T1 cells in the mammary fat pad and treated i.p. with paclitaxel once per week from Day 4 after tumor implantation, alone or in combination with ampicillin that was diluted in drinking water. Two other groups of mice received ampicillin alone or were left untreated.

The antitumor effect of paclitaxel was observable only on combination with ampicillin; no effect was detected with paclitaxel alone (Fig. 9A). Paclitaxel/ampicillin combination did not show signs of an increased liver toxicity as compared to paclitaxel alone, as indicated by no significant change of aspartate aminotransferase plasma level (AST) (Mean pg/ml ± SEM: 446560 ± 28923 in paclitaxel *versus* 519227 ± 48918 in paclitaxel + amp oral) and of liver parenchyma evaluated by histolopathological analysis (not shown).

To confirm that the enhanced antitumor effect of paclitaxel was associated with increased local immune activation, cell suspensions that were obtained by enzymatic digestion of tumor nodules were plated overnight at 37 °C to recover the nonadherent fraction, which harbored immune-infiltrating effector cells. By cytotoxicity assay, the *in vivo* antitumor effect of paclitaxel, when combined with ampicillin, was

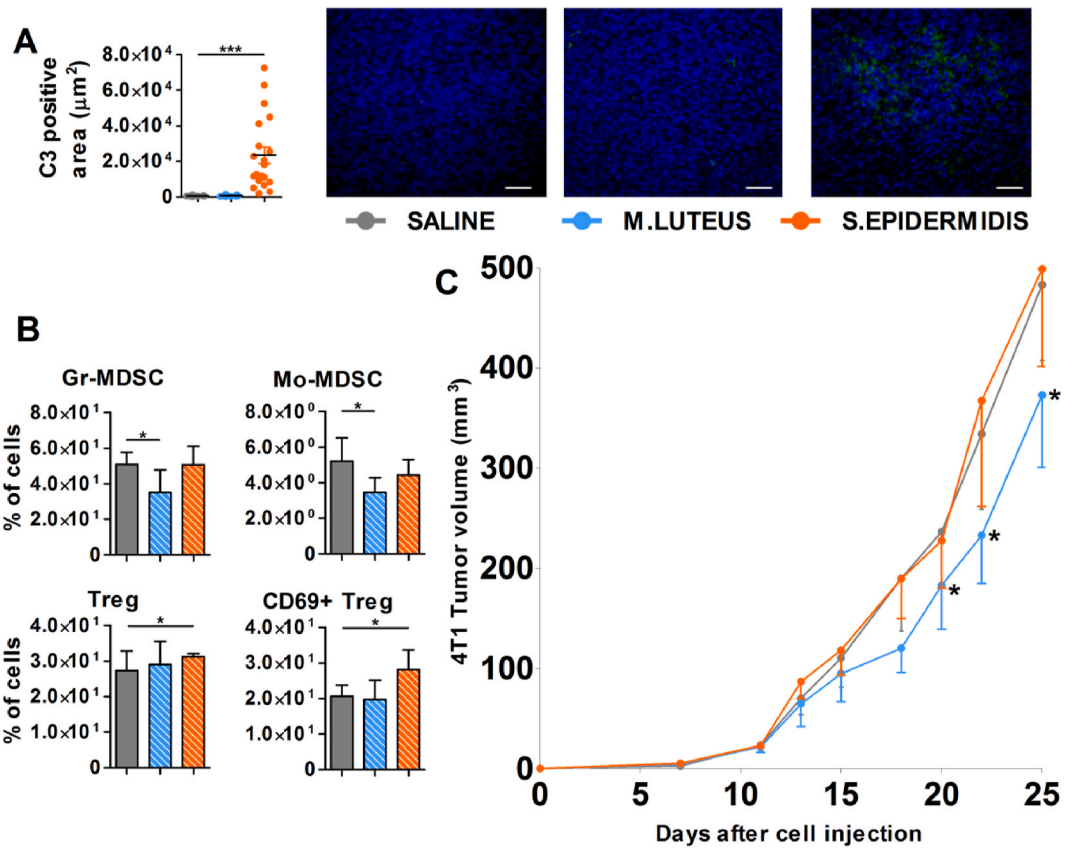

Fig. 8. Effects of bacterial isolates from 4T1 tumor on complement activation, MDSCs, Treg infiltration, and tumor growth.
Mice were injected with 4T1 tumor cells, treated for 10 days with oral ampicillin, and then peritumorally injected with saline, 10^5 CFU Staphylococcus epidermidis, or 10^5 CFU Micrococcus luteus for 7 days. **(A)** Quantification of C3-positive area and representative immunofluorescence photomicrographs of tumor sections obtained at the end of treatment (4 mice/group). Sections were stained for C3 cleavage products (C3b, iC3b, and C3c; green), and nuclei were counterstained with 4′,6-diamidino-2-phenylindole (DAPI; blue). Each dot represents the mean C3-positive area (μm^2) in 2 sections/mouse. Results are expressed as mean C3-positive area ± SEM. The C3-positive area was measured in 5 random fields, acquired using constant parameters. Bars: 40 μm. **(B)** Percentage of Gr-MDSCs ($Ly6c^{low}Ly6g^{+}CD11b^{+}F4/80^{int/low}$), Mo-MDSCs ($Ly6c^{hi}Ly6g^{-}CD11b^{+}F4/80^{int/low}$), Tregs ($CD4^{+}CD25^{+}FoxP3^{+}$), and $CD69^{+}$ Tregs ($CD69^{+}CD4^{+}CD25^{+}FoxP3^{+}$) by FACS analysis of suspensions from digested tumor nodules (5 mice/group). Gating strategies are shown in Suppl. Fig. 5. **(C)** Primary mammary tumor growth, expressed as tumor volume (mean ± SEM); p values are calculated versus saline (6–7 mice/group). *p ≤ 0.05, **p ≤ 0.01, and ***p ≤ 0.001.

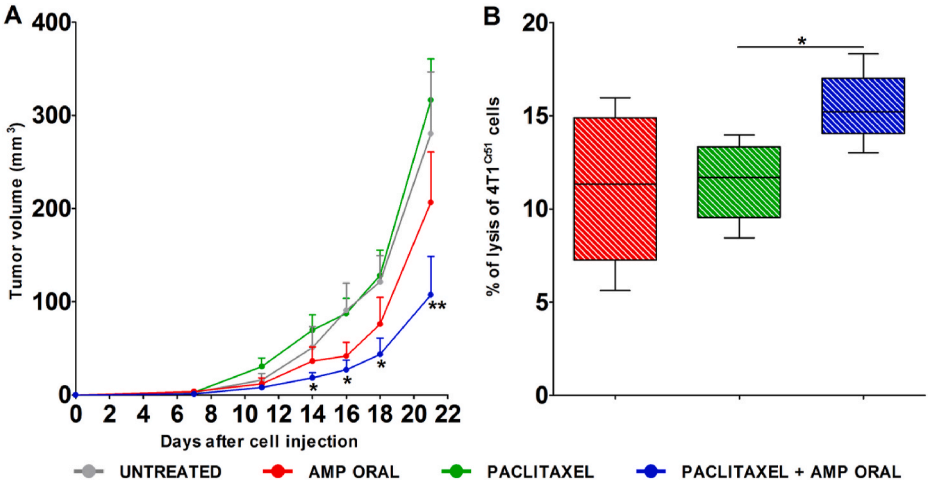

Fig. 9. Effects of oral ampicillin on the response of 4T1 tumors to paclitaxel.
Mice were injected with 4T1 tumor cells into the mammary fat pad and left untreated or treated with i.p. paclitaxel or oral ampicillin alone or with i.p. paclitaxel in combination with oral ampicillin (6–8 mice/group). **(A)** Primary mammary tumor growth, expressed as tumor volume (mean ± SEM); p values for paclitaxel/ampicillin are calculated versus paclitaxel alone. **(B)** Percentage of specific lysis of Cr51-labeled 4T1 target cells cultured for 4 h with nonadherent cells from tumor suspensions of mice treated with paclitaxel alone, ampicillin alone, or paclitaxel/ampicillin (5–6 mice/group). *p ≤ 0.05, **p ≤ 0.01.

associated with significantly greater lysis of ^{51}Cr-labeled 4T1 tumor cells by nonadherent cells (Fig. 9B).

3.7. An amp-like signature defines breast cancer patients with high tumor immune infiltration and a good prognosis

A signature was generated, based on the 8 genes (GABRA6, UHMK1, TENM4, PPM1F, PI16, ARL13A, CARD14, PLCXD3) that discriminate

untreated from amp-treated murine tumors. Applying this signature to the human Metabric breast cancer dataset, we observed an association between Amp-like score and tumor intrinsic subtypes ($p < 0.0001$). Specifically, tumors with Amp-like score (n = 192), compared with untreated-like tumors (n = 53), belonged primarily to the luminal A (30.2% vs 15.1%), claudin-low (30.2% vs 1.9%), and normal-like subtypes (26% vs 0%), whereas luminal B tumors were better represented in the untreated-like group (71.7% vs 3.1%). Untreated-like tumors were mainly ER-positive (92.5% vs 76.6%, $p = 0.0170$) and lymph node-positive (60.4% vs 43.2%, $p = 0.0301$) and had significantly higher Nottingham Prognostic Index scores (NPI, median: 4.07, range: 2.04–6.26 vs median: 4.03, range: 1.02–6.16, $p < 0.0001$).

Remarkably, a significantly better Relapse-Free Survival (RFS) and Overall Survival (OS) were found in Amp-like patients compared to those with an untreated-like tumor in univariate analysis (Fig. 10 A and B). Multivariate analysis by adjusting for variables significantly associated with RFS and OS in univariate analysis [i.e lymph node status, NPI, ER status and the risk of recurrence (ROR-S) score] showed that Amp-like score and NPI were the only features associated with a trend of significance with RFS, while Amp-like score, ER and RORs were significantly associated with OS (Fig. 10A and B). Consistent with the results in 4T1 murine tumors, by GSEA of samples with untreated-like scores, pathways that were related to cell cycle and DNA repair were enriched, compared with Amp-like score samples (Fig. 10B). Amp-like tumors had significantly higher levels of immune cell infiltration, based on immune score (Fig. 10C). Particularly, CD8 T cells, CD4 memory T cells, memory B cells, and monocytes were enriched by CIBERSORTx in these samples; in contrast, M2 and M0 macrophages and T cell follicular helper cell levels were higher in untreated-like samples (Fig. 10D).

Further, a significant correlation was observed between the rate of tumor immune infiltration and a signature of the response to bacteria (Fig. 10E), suggesting that the profile of the local response to bacteria influences immune status in human breast cancers.

4. Discussion

In this study, host treatment with antibiotic reduced the growth of orthotopically implanted mammary tumors by disrupting commensal microorganisms at the tumor site; this effect was limited to oral delivery of absorbable antibiotics—ampicillin or clindamycin—or was induced on peritumoral administration. Consequently, changes in the tumor microbiota remodeled the local immune microenvironment to favor an immune response against the tumor.

Decreased mammary tumor growth was also elicited by the aerosolization of antibiotics, which presumably entered the bloodstream through highly vascularized pulmonary alveoli. Consistent with this hypothesis, aerosolized antibiotics, such as oral ampicillin, shifted the expression of immune genes in the mammary tumor nodules toward an antitumor profile. The antitumor immune profile in oral ampicillin-treated tumors was paralleled by a rise in T lymphocytes and macrophages. In contrast, the number of mast cells declined, supporting emerging evidence of their involvement in host-microbiota communication [39]. This reduction in mice with impaired tumor growth is consistent with studies in mammary tumor models that have implicated mast cells in sustaining tumor growth through the secretion of growth factors, proteases, VEGF, and IL8 [40]. Moreover, the significant decrease in the B cell compartment in ampicillin-treated tumors might be also related to antibiotic-induced changes in the microbial community, as suggested by findings that microbiota can modulate B cells, including immunosuppressive regulatory subsets [41].

The use of antibiotics is associated with an increased risk of developing certain cancers [42], and a growing number of clinical studies have reported the detrimental effects of antibiotic exposure on the response to immunotherapy [43]. Most of these results, however, were obtained in patients who received antibiotic therapy due to an infectious condition that could have *per se* altered the immune response.

Independently of the infectious state, antibiotics might have a conditioning effect on systemic immunity. Recent studies have highlighted that the harmful effects of antibiotics on the response to immunotherapy are strictly related to the timing of administration. A study on melanoma and NSCLC patients reported that prior and early—but not concurrent—antibiotic administration is associated with a worse treatment response and shorter OS [44], and a study in a cohort of hepatocellular carcinoma patients demonstrated that antibiotic treatment 1 month before or after the initiation of immune checkpoint inhibitor (ICI) therapy is linked to a greater benefit from immunotherapy [45]. Antibiotic treatment before chemotherapy also correlates with an increased risk of cancer progression [46]. The detrimental effect of prior and early but not concurrent antibiotic use in malignancies is believed to be related to their negative effect on the gut microbiota, causing specific depletion of *Bifidobacterium* spp, *Akkermansia,* and *Ruminococcus*, which have been associated with increased immune activation, while favoring the growth of other taxa, such as *Bacteroides*, that have been postulated to induce immunosuppression by promoting myeloid-derived suppressor cells and $FOXP3^+$ and $CD4^+CD25^+$ Tregs [47].

Thus, adverse effects on systemic immune control of tumor growth or the response to therapy likely prevail when severe or long-lasting early antibiotic therapy heavily impacts the intestinal microbiota, affecting its ability to prime the immune system. In contrast, concomitant or milder therapy that has a seemingly lower impact on the gut can be beneficial by preventing, in tumoral tissue, the overgrowth of inflammatory or immunosuppressive bacterial species that are typically recruited to the tumor microenvironment. Accordingly, recent findings have demonstrated that microorganisms in and adjacent to tumors affect cancer progression in lung and pancreatic disease by dampening local immune responses [3–5], implicating the tumor-associated microbiota in subverting the local immune microenvironment.

Consistent with the literature, in which tumors have a distinct microbiome composition *versus* their respective healthy tissue [2], we observed that the growth of 4T1 tumor cells in the mammary fat pad of mice reshaped the microbiota in the mammary gland, as evidenced by the decrease in OTU richness and changes in the presence or abundance of bacterial taxa. Oral antibiotic treatment did not considerably affect OTU richness but significantly altered certain taxa, 2 of which were enriched in untreated tumors, with the remaining taxa expanded in antibiotic-treated nodules, reshaping the tumor microbiota by antibiotic but not effecting suppression. In parallel, by culture, we confirmed that the microbial DNA in tumoral tissues was actively derived from viable bacterial cells that were growing in the mammary gland—species that we identified by MALDI TOF as being consistent with the taxa that were detected in the metagenomic analysis. Notably, we can exclude an effect of ampicillin, which is unable to penetrate cells, on intracellular bacteria, the role of which in tumor progression has been recently highlighted in murine breast cancer [48].

Bacteria that are typically associated with the skin, such as *S. epidermidis* and *M. luteus*, have been isolated from mammary tumors [10,11], as expected, considering that skin bacteria can access the mammary ducts through the nipple and spread within the mammary glands through lobules and ducts. Consistent with our findings, in a study of breast tissue from women who were undergoing surgery for breast reduction or tumor excision, Urbaniak et al. observed a clear distinction of microbiome profiles between healthy and malignant tissue and reported *Staphylococcus* spp as one of the most abundant genera in cancer patients, whereas *Micrococcus* spp abounds in healthy individuals [11]. The presence of *S. epidermidis* in the breast has also been demonstrated in a pioneering study of coccoid forms in primary breast and metastatic lesions [49].

Whereas Urbaniak et al. ascribed the carcinogenic activity of *S. epidermidis* to its ability to induce DNA damage in HeLa cells [11], our results identify a novel mechanism that describes *S. epidermidis* as a strong inducer of inflammation that, in turn, promotes cancer progression. I*n vitro* studies have shown that coculture of BMDMs with an

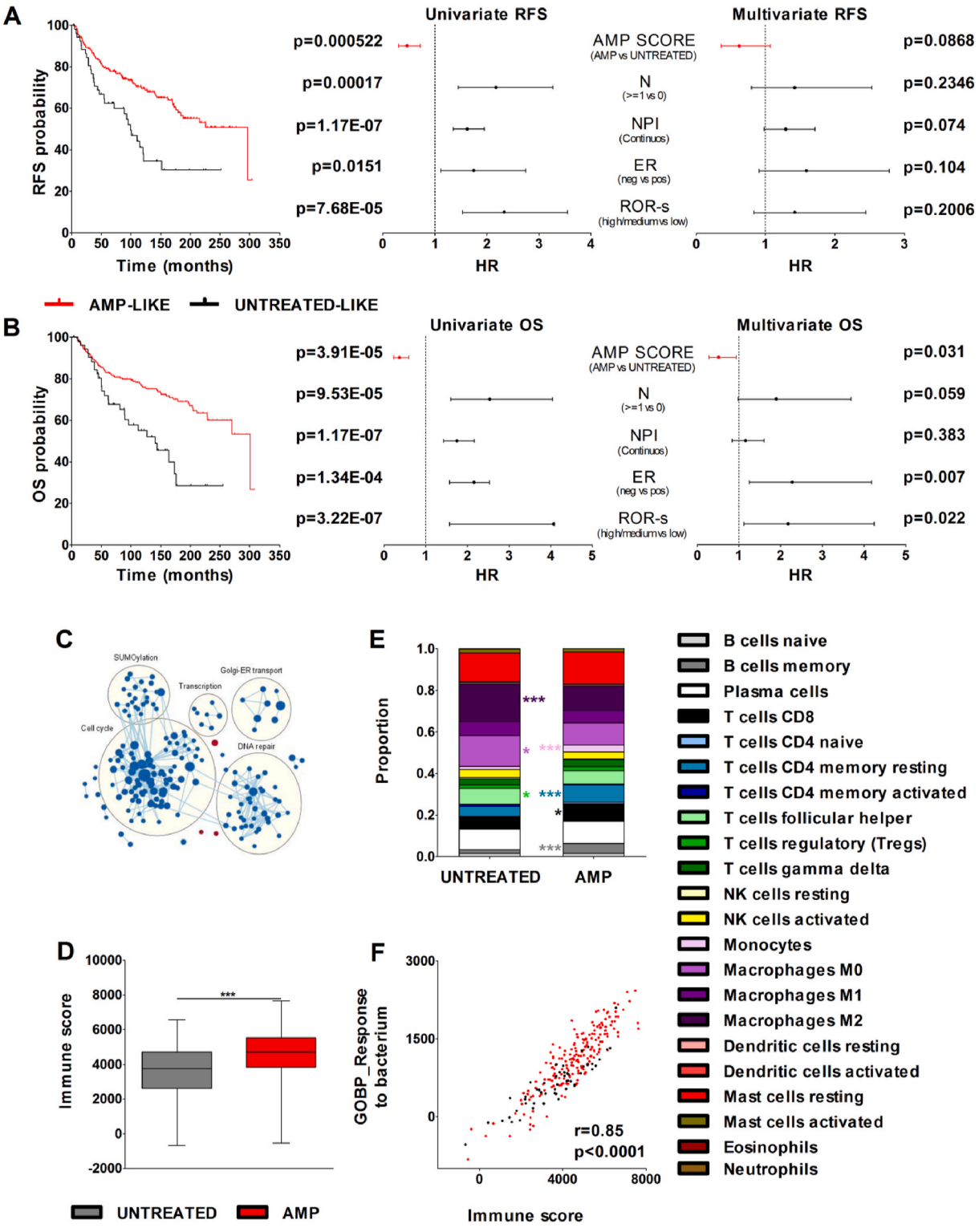

Fig. 10. Evaluation of Amp score in the Metabric human breast cancer dataset.
(A) Association between Amp-like (red, n = 192) and untreated-like (black, n = 53) patients with relapse-free survival (RFS) in Metabric dataset and effect of Amp score, clinicopathological variables and other signatures on RFS in a univariate and multivariate analyses. **(B)** Association between Amp-like (red, n = 192) and untreated-like (black, n = 53) patients with overall survival (OS) in Metabric dataset and effect of Amp score, clinicopathological variables and other signatures on OS in a univariate and multivariate analyses. Symbols used in A and B indicate hazard ratio (HR), and error bars 95% confidence interval (CI). Abbreviations: N = lymph node; NPI = Nottingham Prognostic Index, ER = estrogen receptor, ROR-s = Risk of Relapse by Subtype along. **(C)** Enrichment Map of Reactome pathways that are significantly enriched ($p < 0.05$, FDR < 0.1) in untreated-like (blue circles) versus Amp-like (red circles) human tumors from Metabric dataset by GSEA. Only clusters containing at least 4 gene sets are visualized. **(D)** Immune score levels according to Amp score. p-value by unpaired t-test. **(E)** Average relative fractions of 22 leukocyte subtypes (LM22 signature) as computed by CIBERSORTx in the untreated-like and amp-like subgroups. The asterisks indicate the significant differentially enriched immune infiltrated cells in the two groups. *$p \leq 0.05$, ***$p \leq 0.001$. **(F)** Samples of the Metabric dataset classified according to their immune score and a signature of response to bacteria and colored according to their amp score (Amp-like: red; Untreated-like: black). r di Pearson and relative p-value are shown.

S. epidermidis strain from 4T1 tumors effects the release of proinflammatory cytokines and chemokines, paralleling the upregulation of Irf4, an M2 transcription factor. Moreover, *S. epidermidis* also increases the deposition of C3 cleavage products in tumor nodules, and accordingly, complement activation has emerged as a tumor-promoting pathway, inducing tumor inflammation and immunosuppression [50]. Magrini et al. have observed C3 activation in murine sarcoma models via the recognition of aberrant glycosylation patterns on tumor cells through the classical or lectin pathway [50].

Thus, our results indicate that even bacteria that are recruited to tumoral tissue contribute to tumoral complement activation. In contrast to the effects of *S. epidermidis*, the lower inflammatory activity of *M. luteus* was associated with the upregulation of M1-related genes. These effects explain the ability of *M. luteus* to reduce 4T1 tumor growth when transferred peritumorally. Conversely, no effect was observed on transfer of *S. epidermidis*, which overgrew in untreated tumors.

In combination with oral ampicillin, the robust antitumor efficacy of paclitaxel, which is administered to breast cancer patients, is likely attributed to the shift in microbial species in the tumor that synergize with it in inducing an immune profile that favors an anticancer response. Consistent with this hypothesis, the cytotoxic activity of tumor-infiltrating cells was greater in mice that were treated with paclitaxel plus ampicillin *versus* paclitaxel alone. Paclitaxel alone did not affect 4T1 triple-negative tumor growth, as reported in the same murine model, showing antitumor activity only in combination regimens [51, 52]. Our results suggest that concomitant antibiotic treatment is suitable for combination with other immunotherapeutic drugs, such as immune checkpoint inhibitors, which have recently been evaluated in metastatic triple-negative breast cancer (TNBC) trials [53], to disrupt microbes in the tumoral tissue and prevent the overgrowth of bacteria with inflammatory or immunosuppressive effects.

With regard to translational medicine, these findings might lead to the introduction of short-course oral antibiotic exposure during each chemotherapeutic/immunotherapeutic treatment or the development of local antibiotic delivery strategies, such as nanoparticles and liposomes, for combination with conventional therapies in TNBC. Based on differences in tumor microbiota relative to breast cancer subtypes [13], further studies are needed to define whether antibiotic treatment is effective in all or specific breast cancer subtypes. The association between the Amp-like phenotype, which is characterized by genes that are involved in the microbial signaling or associated with the response to specific bacteria (GABRA6, PPM1F, CARD14 and UHMK1) [54–57], and a significantly better OS in the univariate and multivariate analyses in the Metabric dataset suggests that patients with the Amp-like phenotype have an intrinsically favorable tumor microbiota.

Amp-like breast cancers were infiltrated by more immune cells, and their immune scores correlated with a of the response to bacteria, reinvigorating the idea that the presence of certain bacteria in a tumor might influences the immune status. Thus, further studies are needed to dissect the microbial composition of human breast tumors and link specific bacteria to the immune infiltrate.

Our findings highlight a clear and crucial function of the microbiota that colonizes the mammary tumor in shaping the immune microenvironment. Moreover, our results reveal that antibiotic treatment during tumor development disrupts the composition of tumoral tissue-residing bacteria, shifting the balance between those that induce tumor-promoting inflammation and those that guide antitumor immune activities. Overall, our data reveal an unappreciated effect of antibiotics as a potent tool for targeting the tumor immune microenvironment during cancer treatment and promoting an effective antitumor immune response.Overall, these data suggest that oral ampicillin treatment is associated with changes in microbial signaling in mammary tumoral tissue.

Author contributions

Giancarla Bernardo: Methodology, Investigation, Visualization; **Valentino Le Noci**: Methodology, Investigation, Visualization; **Emerenziana Ottaviano**: Methodology, Investigation, Visualization; **Loris De Cecco**: Investigation; **Chiara Camisaschi**: Methodology, Investigation, Writing- review and editing, Visualization; **Simone Guglielmetti**: Investigation, Writing- review and editing; **Martina Di Modica**: Methodology; **Giorgio Gargari**: Investigation; **Francesca Bianchi**: Methodology; **Serena Indino**: Methodology; **Patrizia Sartori**: Methodology; **Elisa Borghi**: Investigation, Writing- review and editing; **Michele Sommariva:** Investigation, Writing- review and editing; **Elda Tagliabue**: Conceptualization, Writing- original draft Writing- review and editing, Supervision; **Tiziana Triulzi**: Investigation, Writing- original draft, Writing- review and editing; **and Lucia Sfondrini**: Conceptualization, Methodology, Investigation, Writing- original draft, Writing-review and editing, Supervision, Funding Acquisition.

Funding

The research leading to this manuscript has received funding from AIRC under IG 2020 – ID. 24718 project – PI Sfondrini Lucia and from Piano di Sostegno alla Ricerca 2019, Università degli Studi di Milano.

Declaration of competing interest

The authors declare no potential conflicts of interest.

Acknowledgments

We thank Dr. Mario P. Colombo for providing the N2C mammary tumor cell line, Dr. Elena Vezzoli for technical support in analyzing MCs in tumor specimens, Dr. Viola Regondi for technical preparation of liver sections and Dr. Giuseppe Leoncini, pathologist, for their histopathological evaluation.

The research leading to these results has received funding from AIRC under IG 2020 - ID. 24718 project – P.I. Lucia Sfondrini and from Piano di Sostegno alla Ricerca Linea 2 2019 Università degli Studi di Milano – P.I. Lucia Sfondrini.

Appendix A. Supplementary data

Supplementary data to this article can be found online at https://doi.org/10.1016/j.canlet.2022.216041.

References

[1] R. Salihoglu, T. Onal-Suzek, Tissue microbiome associated with human diseases by whole transcriptome sequencing and 16S metagenomics, Front. Genet. 12 (2021), 585556.

[2] D. Nejman, I. Livyatan, G. Fuks, N. Gavert, Y. Zwang, L.T. Geller, A. Rotter-Maskowitz, R. Weiser, G. Mallel, E. Gigi, A. Meltser, G.M. Douglas, I. Kamer, V. Gopalakrishnan, T. Dadosh, S. Levin-Zaidman, S. Avnet, T. Atlan, Z.A. Cooper, R. Arora, A.P. Cogdill, M.A.W. Khan, G. Ologun, Y. Bussi, A. Weinberger, M. Lotan-Pompan, O. Golani, G. Perry, M. Rokah, K. Bahar-Shany, E.A. Rozeman, C.U. Blank, A. Ronai, R. Shaoul, A. Amit, T. Dorfman, R. Kremer, Z.R. Cohen, S. Harnof, T. Siegal, E. Yehuda-Shnaidman, E.N. Gal-Yam, H. Shapira, N. Baldini, M.G. I. Langille, A. Ben-Nun, B. Kaufman, A. Nissan, T. Golan, M. Dadiani, K. Levanon, J. Bar, S. Yust-Katz, I. Barshack, D.S. Peeper, D.J. Raz, E. Segal, J.A. Wargo, J. Sandbank, N. Shental, R. Straussman, The human tumor microbiome is composed of tumor type-specific intracellular bacteria, Science 368 (2020) 973–980.

[3] V. Le Noci, S. Guglielmetti, S. Arioli, C. Camisaschi, F. Bianchi, M. Sommariva, C. Storti, T. Triulzi, C. Castelli, A. Balsari, E. Tagliabue, L. Sfondrini, Modulation of pulmonary microbiota by antibiotic or probiotic aerosol therapy: a strategy to promote immunosurveillance against lung metastases, Cell Rep. 24 (2018) 3528–3538.

[4] S. Pushalkar, M. Hundeyin, D. Daley, C.P. Zambirinis, E. Kurz, A. Mishra, N. Mohan, B. Aykut, M. Usyk, L.E. Torres, G. Werba, K. Zhang, Y. Guo, Q. Li, N. Akkad, S. Lall, B. Wadowski, J. Gutierrez, J.A. Kochen Rossi, J.W. Herzog, B. Diskin, A. Torres-Hernandez, J. Leinwand, W. Wang, P.S. Taunk, S. Savadkar, M. Janal, A. Saxena, X. Li, D. Cohen, R.B. Sartor, D. Saxena, G. Miller, The

pancreatic cancer microbiome promotes oncogenesis by induction of innate and adaptive immune suppression, Cancer Discov. 8 (2018) 403–416.
[5] C. Jin, G.K. Lagoudas, C. Zhao, S. Bullman, A. Bhutkar, B. Hu, S. Ameh, D. Sandel, X.S. Liang, S. Mazzilli, M.T. Whary, M. Meyerson, R. Germain, P.C. Blainey, J. G. Fox, T. Jacks, Commensal microbiota promote lung cancer development via gammadelta T cells, Cell 176 (2019) 998–1013.
[6] S. Parida, S. Wu, S. Siddharth, G. Wang, N. Muniraj, A. Nagalingam, C. Hum, P. Mistriotis, H. Hao, C.C. Talbot Jr., K. Konstantopoulos, K.L. Gabrielson, C. L. Sears, D. Sharma, A procarcinogenic colon microbe promotes breast tumorigenesis and metastatic progression and concomitantly activates notch and i^2-catenin axes, Cancer Discov. 11 (2021) 1138–1157.
[7] C.L. Sears, A.L. Geis, F. Housseau, Bacteroides fragilis subverts mucosal biology: from symbiont to colon carcinogenesis, J. Clin. Invest. 124 (2014) 4166–4172.
[8] K. Zhao, Y. Hu, Microbiome harbored within tumors: a new chance to revisit our understanding of cancer pathogenesis and treatment, Signal Transduct. Targeted Ther. 5 (2020) 136.
[9] L. Fernandez, P.S. Pannaraj, S. Rautava, J.M. Rodriguez, The microbiota of the human mammary ecosystem, Front. Cell. Infect. Microbiol. 10 (2020), 586667.
[10] C. Urbaniak, J. Cummins, M. Brackstone, J.M. Macklaim, G.B. Gloor, C.K. Baban, L. Scott, D.M. O'Hanlon, J.P. Burton, K.P. Francis, M. Tangney, G. Reid, Microbiota of human breast tissue, Appl. Environ. Microbiol. 80 (2014) 3007–3014.
[11] C. Urbaniak, G.B. Gloor, M. Brackstone, L. Scott, M. Tangney, G. Reid, The microbiota of breast tissue and its association with breast cancer, Appl. Environ. Microbiol. 82 (2016) 5039–5048.
[12] T.J. Hieken, J. Chen, T.L. Hoskin, M. Walther-Antonio, S. Johnson, S. Ramaker, J. Xiao, D.C. Radisky, K.L. Knutson, K.R. Kalari, J.Z. Yao, L.M. Baddour, N. Chia, A. C. Degnim, The microbiome of aseptically collected human breast tissue in benign and malignant disease, Sci. Rep. 6 (2016), 30751.
[13] S. Banerjee, T. Tian, Z. Wei, N. Shih, M.D. Feldman, K.N. Peck, A.M. DeMichele, J. C. Alwine, E.S. Robertson, Distinct microbial signatures associated with different breast cancer types, Front. Microbiol. 9 (2018) 951.
[14] F. Aragon, S. Carino, G. Perdigon, A. de Moreno de LeBlanc, Inhibition of growth and metastasis of breast cancer in mice by milk fermented with Lactobacillus casei CRL 431, J. Immunother. 38 (2015) 185–196.
[15] L. Parhi, T. Alon-Maimon, A. Sol, D. Nejman, A. Shhadeh, T. Fainsod-Levi, O. Yajuk, B. Isaacson, J. Abed, N. Maalouf, A. Nissan, J. Sandbank, E. Yehuda-Shnaidman, F. Ponath, J. Vogel, O. Mandelboim, Z. Granot, R. Straussman, G. Bachrach, Breast cancer colonization by Fusobacterium nucleatum accelerates tumor growth and metastatic progression, Nat. Commun. 11 (2020) 3259–16967.
[16] V. Le Noci, G. Bernardo, F. Bianchi, E. Tagliabue, M. Sommariva, L. Sfondrini, Toll like receptors as sensors of the tumor microbial dysbiosis: implications in cancer progression, Front. Cell Dev. Biol. 9 (2021), 732192.
[17] C. Denkert, S. Loibl, A. Noske, M. Roller, B.M. Muller, M. Komor, J. Budczies, S. Darb-Esfahani, R. Kronenwett, C. Hanusch, C. von Torne, W. Weichert, K. Engels, C. Solbach, I. Schrader, M. Dietel, G. Von Minckwitz, Tumor-associated lymphocytes as an independent predictor of response to neoadjuvant chemotherapy in breast cancer, J. Clin. Oncol. 28 (2010) 105–113.
[18] M.R. Shurin, H. Naiditch, D.W. Gutkin, V. Umansky, G.V. Shurin, ChemoImmunoModulation: immune regulation by the antineoplastic chemotherapeutic agents, Curr. Med. Chem. 19 (2012) 1792–1803.
[19] S. Sangaletti, A. Stoppacciaro, C. Guiducci, M.R. Torrisi, M.P. Colombo, Leukocyte, rather than tumor-produced SPARC, determines stroma and collagen type IV deposition in mammary carcinoma, J. Exp. Med. 198 (2003) 1475–1485.
[20] M. Sommariva, V. Le Noci, C. Storti, F. Bianchi, E. Tagliabue, A. Balsari, L. Sfondrini, Activation of NK cell cytotoxicity by aerosolized CpG-ODN/poly(I:C) against lung melanoma metastases is mediated by alveolar macrophages, Cell. Immunol. 313 (2017) 52–58.
[21] F. Bianchi, M. Sommariva, V. Le Noci, S. Camelliti, N. Gagliano, M. Giussani, A. Balsari, E. Tagliabue, L. Sfondrini, Aerosol 1,25-dihydroxyvitamin D3 supplementation: a strategy to boost anti-tumor innate immune activity, PLoS One 16 (2021), e0248789.
[22] J. Lluch, F. Servant, S. Paisse, C. Valle, S. Valiere, C. Kuchly, G. Vilchez, C. Donnadieu, M. Courtney, R. Burcelin, J. Amar, O. Bouchez, B. Lelouvier, The characterization of novel tissue microbiota using an optimized 16S metagenomic sequencing pipeline, PLoS One 10 (2015), e0142334.
[23] S. Guglielmetti, S. Bernardi, C. Del Bo, A. Cherubini, M. Porrini, G. Gargari, N. Hidalgo-Liberona, R. Gonzalez-Dominguez, G. Peron, R. Zamora-Ros, M. S. Winterbone, B. Kirkup, P.A. Kroon, C. ndres-Lacueva, P. Riso, Effect of a polyphenol-rich dietary pattern on intestinal permeability and gut and blood microbiomics in older subjects: study protocol of the MaPLE randomised controlled trial, BMC Geriatr. 20 (2020) 77–1472.
[24] C. Pellaton, S. Nutten, A.C. Thierry, C. Boudousquie, N. Barbier, C. Blanchard, B. Corthesy, A. Mercenier, F. Spertini, Intragastric and intranasal administration of Lactobacillus paracasei NCC2461 modulates allergic airway inflammation in mice, 2012, Int. J. Inflamm. (2012), 686739, https://doi.org/10.1155/2012/686739.
[25] A. Martinetti, R. Miceli, E. Sottotetti, M. Di Bartolomeo, F. De Braud, A. Gevorgyan, K.F. Dotti, E. Bajetta, M. Campiglio, F. Bianchi, G. Bregni, F. Pietrantonio, Circulating biomarkers in advanced colorectal cancer patients randomly assigned to three bevacizumab-based regimens, Cancers 6 (2014) 1753–1768.
[26] E.J. Breen, W. Tan, A. Khan, The statistical value of raw fluorescence signal in luminex xMAP based multiplex immunoassays, Sci. Rep. 6 (2016), 26996.
[27] S. Camelliti, V. Le Noci, F. Bianchi, C. Storti, F. Arnaboldi, A. Cataldo, S. Indino, E. Jachetti, M. Figini, M.P. Colombo, A. Balsari, N. Gagliano, E. Tagliabue, L. Sfondrini, M. Sommariva, Macrophages impair TLR9 agonist antitumor activity through interacting with the anti-PD-1 antibody Fc domain, Cancers 13 (2021) 4081.
[28] A. Subramanian, P. Tamayo, V.K. Mootha, S. Mukherjee, B.L. Ebert, M.A. Gillette, A. Paulovich, S.L. Pomeroy, T.R. Golub, E.S. Lander, J.P. Mesirov, Gene set enrichment analysis: a knowledge-based approach for interpreting genome-wide expression profiles, Proc. Natl. Acad. Sci. U.S.A. 102 (2005) 15545–15550.
[29] J. Friedman, T. Hastie, R. Tibshirani, Regularization paths for generalized linear models via coordinate descent, J Stat.Softw. 33 (2010) 1–22.
[30] K. Yoshihara, M. Shahmoradgoli, E. Martinez, R. Vegesna, H. Kim, W. Torres-Garcia, V. Trevino, H. Shen, P.W. Laird, D.A. Levine, S.L. Carter, G. Getz, K. Stemke-Hale, G.B. Mills, R.G. Verhaak, Inferring tumour purity and stromal and immune cell admixture from expression data, Nat. Commun. 4 (2013) 2612.
[31] M.I. Love, W. Huber, S. Anders, Moderated estimation of fold change and dispersion for RNA-seq data with DESeq2, Genome Biol. 15 (2014) 550.
[32] A. Aponte-Lopez, E.M. Fuentes-Panana, D. Cortes-Munoz, S. Munoz-Cruz, Mast cell, the neglected member of the tumor microenvironment: role in breast cancer, 2018, J. Immunol. Res. (2018), 2584243.
[33] M. Sommariva, L. De Cecco, M. De Cesare, L. Sfondrini, S. Ménard, C. Melani, D. Delia, N. Zaffaroni, G. Pratesi, V. Uva, E. Tagliabue, A. Balsari, TLR9-agonists oppositely modulate DNA-repair genes in tumor vesus immune cells and ehance chemotherapy effects, Cancer Res. 71 (2011) 6382–6390.
[34] D.C. Zysset-Burri, I. Keller, L.E. Berger, C.R. Largiadèr, M. Wittwer, S. Wolf, M. S. Zinkernagel, Associations of the intestinal microbiome with the complement system in neovascular age-related macular degeneration, NPJ.Genom.Med. 5 (2020) 34.
[35] E.G. Fredheim, H.N. Granslo, T. Flaegstad, Y. Figenschau, H. Rohde, I. Sadovskaya, T.E. Mollnes, C. Klingenberg, Staphylococcus epidermidis polysaccharide intercellular adhesin activates complement, FEMS Immunol. Med. Microbiol. 63 (2011) 269–280.
[36] M. Bosiljcic, R.A. Cederberg, M.J. Hamilton, N.E. LePard, B.T. Harbourne, J. L. Collier, E.C. Halvorsen, R. Shi, S.E. Franks, A.Y. Kim, J.P. BanÃ¡th, M. Hamer, F. M. Rossi, K.L. Bennewith, Targeting myeloid-derived suppressor cells in combination with primary mammary tumor resection reduces metastatic growth in the lungs, Breast Cancer Res. 21 (2019) 103–1189.
[37] L. Yu, F. Yang, F. Zhang, D. Guo, L. Li, X. Wang, T. Liang, J. Wang, Z. Cai, H. Jin, CD69 enhances immunosuppressive function of regulatory T-cells and attenuates colitis by prompting IL-10 production, Cell Death Dis. 9 (2018), 905-0927.
[38] C.W. Wanderley, D.F. Colon, J.P.M. Luiz, F.F. Oliveira, P.R. Viacava, C.A. Leite, J. A. Pereira, C.M. Silva, C.R. Silva, R.L. Silva, C.A. Speck-Hernandez, J.M. Mota, J. C. Alves-Filho, R.C. Lima-Junior, T.M. Cunha, F.Q. Cunha, Paclitaxel reduces tumor growth by reprogramming tumor-associated macrophages to an M1 profile in a TLR4-dependent manner, Cancer Res. 78 (2018) 5891–5900.
[39] M. De Zuani, C. Dal Secco, B. Frossi, Mast cells at the crossroads of microbiota and IBD, Eur. J. Immunol. 48 (2018) 1929–1937.
[40] P. Conti, M.L. Castellani, D. Kempuraj, V. Salini, J. Vecchiet, S. Tetè, F. Mastrangelo, A. Perrella, M.A. De Lutiis, M. Tagen, T.C. Theoharides, Role of mast cells in tumor growth, Ann. Clin. Lab. Sci. 37 (2007) 315–322.
[41] E.C. Rosser, K. Oleinika, S. Tonon, R. Doyle, A. Bosma, N.A. Carter, K.A. Harris, S. A. Jones, N. Klein, C. Mauri, Regulatory B cells are induced by gut microbiota-driven interleukin-1i^2 and interleukin-6 production, Nat. Med. 20 (2014) 1334–1339.
[42] B. Boursi, R. Mamtani, K. Haynes, Y.X. Yang, Recurrent antibiotic exposure may promote cancer formation–Another step in understanding the role of the human microbiota?, Oxford, England : 1990, Eur. J. Cancer 51 (2015) 2655–2664.
[43] A. Elkrief, L. Derosa, G. Kroemer, L. Zitvogel, B. Routy, The negative impact of antibiotics on outcomes in cancer patients treated with immunotherapy: a new independent prognostic factor? Ann. Oncol. 30 (2019) 1572–1579.
[44] A.F. Nyein, S. Bari, S. Hogue, Y. Zhao, B. Maller, S. Sha, M.F. Gomez, D.E. Rollison, L.A. Robinson, Effect of prior antibiotic or chemotherapy treatment on immunotherapy response in non-small cell lung cancer, BMC Cancer 22 (2022) 101.
[45] P. Fessas, M. Naeem, M. Pinter, T.U. Marron, D. Szafron, L. Balcar, A. Saeed, T. Jun, S. Dharmapuri, A. Gampa, Y. Wang, U. Khan, M. Muzaffar, M. Navaid, P.C. Lee, A. Bulumulle, B. Yu, S. Paul, N. Nimkar, D. Bettinger, H. Hildebrand, Y.I. Abugabal, T. Pressiani, N. Personeni, N. Nishida, M. Kudo, A. Kaseb, Y.H. Huang, C. Ang, A. Pillai, L. Rimassa, A.R. Naqash, E. Sharon, A. Cortellini, D.J. Pinato, Early antibiotic exposure is not detrimental to therapeutic effect from immunotherapy in hepatocellular carcinoma, Liver Cancer 10 (2021) 583–592.
[46] S. Viaud, F. Saccheri, G. Mignot, T. Yamazaki, R. Daillere, D. Hannani, D.P. Enot, C. Pfirschke, C. Engblom, M.J. Pittet, A. Schlitzer, F. Ginhoux, L. Apetoh, E. Chachaty, P.L. Woerther, G. Eberl, M. Berard, C. Ecobichon, D. Clermont, C. Bizet, V. Gaboriau-Routhiau, N. Cerf-Bensussan, P. Opolon, N. Yessaad, E. Vivier, B. Ryffel, C.O. Elson, J. Dore, G. Kroemer, P. Lepage, I.G. Boneca, F. Ghiringhelli, L. Zitvogel, The intestinal microbiota modulates the anticancer immune effects of cyclophosphamide, Science 342 (2013) 971–976, https://doi.org/10.1126/science.1240537.
[47] V. Gopalakrishnan, C.N. Spencer, L. Nezi, A. Reuben, M.C. Andrews, T. V. Karpinets, P.A. Prieto, D. Vicente, K. Hoffman, S.C. Wei, A.P. Cogdill, L. Zhao, C. W. Hudgens, D.S. Hutchinson, T. Manzo, M. Petaccia de Macedo, T. Cotechini, T. Kumar, W.S. Chen, S.M. Reddy, R. Szczepaniak Sloane, J. Galloway-Pena, H. Jiang, P.L. Chen, E.J. Shpall, K. Rezvani, A.M. Alousi, R.F. Chemaly, S. Shelburne, L.M. Vence, P.C. Okhuysen, V.B. Jensen, A.G. Swennes, F. McAllister, E. Marcelo Riquelme Sanchez, Y. Zhang, E. Le Chatelier, L. Zitvogel, N. Pons, J. L. Austin-Breneman, L.E. Haydu, E.M. Burton, J.M. Gardner, E. Sirmans, J. Hu, A. J. Lazar, T. Tsujikawa, A. Diab, H. Tawbi, I.C. Glitza, W.J. Hwu, S.P. Patel, S. E. Woodman, R.N. Amaria, M.A. Davies, J.E. Gershenwald, P. Hwu, J.E. Lee, J. Zhang, L.M. Coussens, Z.A. Cooper, P.A. Futreal, C.R. Daniel, N.J. Ajami, J. F. Petrosino, M.T. Tetzlaff, P. Sharma, J.P. Allison, R.R. Jenq, J.A. Wargo, Gut

microbiome modulates response to anti-PD-1 immunotherapy in melanoma patients, Science 359 (2018) 97–103.
[48] A. Fu, B. Yao, T. Dong, Y. Chen, J. Yao, Y. Liu, H. Li, H. Bai, X. Liu, Y. Zhang, C. Wang, Y. Guo, N. Li, S. Cai, Tumor-resident intracellular microbiota promotes metastatic colonization in breast cancer, Cell 185 (2022) 1356–1372.
[49] A.R. Cantwell Jr., D.W. Kelso, Microbial findings in cancers of the breast and in their metastases to the skin. Implications for etiology, J. Dermatol. Surg. Oncol. 7 (1981) 483–491.
[50] E. Magrini, S. Di Marco, S.N. Mapelli, C. Perucchini, F. Pasqualini, A. Donato, M. de la Luz Guevara Lopez, R. Carriero, A. Ponzetta, P. Colombo, F. Cananzi, D. Supino, E.S. Reis, C. Peano, A. Inforzato, S. Jaillon, A. Doni, J.D. Lambris, A. Mantovani, C. Garlanda, Complement activation promoted by the lectin pathway mediates C3aR-dependent sarcoma progression and immunosuppression, Nat. Can. (Que.) 2 (2021) 218–232.
[51] P. Falvo, S. Orecchioni, R. Hillje, A. Raveane, P. Mancuso, C. Camisaschi, L. Luzi, P. Pelicci, F. Bertolini, Cyclophosphamide and vinorelbine activate stem-like CD8(+) T cells and improve anti-PD-1 efficacy in triple-negative breast cancer, Cancer Res. 81 (2021) 685–697.
[52] J. Su, D. Li, Q. Chen, M. Li, L. Su, T. Luo, D. Liang, G. Lai, O. Shuai, C. Jiao, Q. Wu, Y. Xie, X. Zhou, Anti-breast cancer enhancement of a polysaccharide from spore of ganoderma lucidum with paclitaxel: suppression on tumor metabolism with gut microbiota reshaping, Front. Microbiol. 9 (2018) 3099.
[53] D. Miles, J. Gligorov, F. André, D. Cameron, A. Schneeweiss, C. Barrios, B. Xu, A. Wardley, D. Kaen, L. Andrade, V. Semiglazov, M. Reinisch, S. Patel, M. Patre, L. Morales, S.L. Patel, M. Kaul, T. Barata, J. O'Shaughnessy, Primary results from IMpassion131, a double-blind, placebo-controlled, randomised phase III trial of first-line paclitaxel with or without atezolizumab for unresectable locally advanced/metastatic triple-negative breast cancer, Ann. Oncol. 32 (2021) 994–1004.
[54] J.K. Kim, Y.S. Kim, H.M. Lee, H.S. Jin, C. Neupane, S. Kim, S.H. Lee, J.J. Min, M. Sasai, J.H. Jeong, S.K. Choe, J.M. Kim, M. Yamamoto, H.E. Choy, J.B. Park, E. K. Jo, GABAergic signaling linked to autophagy enhances host protection against intracellular bacterial infections, Nat. Commun. 9 (2018), 4184-06487.
[55] C. Zhang, X. Han, L. Yang, J. Fu, C. Sun, S. Huang, W. Xiao, Y. Gao, Q. Liang, X. Wang, F. Luo, W. Lu, Y. Zhou, Circular RNA circPPM1F modulates M1 macrophage activation and pancreatic islet inflammation in type 1 diabetes mellitus, Theranostics 10 (2020) 10908–10924.
[56] I. Scudiero, P. Mazzone, L.E. D'Andrea, A. Ferravante, T. Zotti, G. Telesio, G. De Rubis, C. Reale, M. Pizzulo, S. Muralitharan, P. Vito, R. Stilo, CARMA2sh and ULK2 control pathogen-associated molecular patterns recognition in human keratinocytes: psoriasis-linked CARMA2sh mutants escape ULK2 censorship, Cell Death Dis. 8 (2017) e2627.
[57] X. Feng, D. Ma, J. Zhao, Y. Song, Y. Zhu, Q. Zhou, F. Ma, X. Liu, M. Zhong, Y. Liu, Y. Xiong, X. Qiu, Z. Zhang, H. Zhang, Y. Zhao, K. Zhang, X. Hong, Z. Zhang, UHMK1 promotes gastric cancer progression through reprogramming nucleotide metabolism, EMBO J. 39 (2020), e102541.